8 Yarn Tensions and Balloon Geometry in Ring Spinning and Winding

8.1 INTRODUCTION

The basic principles of ring spinning were described in Chapter 6, and it was explained that, as the traveler circulates the ring, it pulls with it the yarn length between the pigtail lappet guide and the traveler. This length circulates the axis common to the spindle, ring, and lappet guide. In doing so, the yarn length balloons, and the tension, air-drag, and the inertial, central, and Coriolis forces acting on the yarn length govern the balloon geometry.

In winding, discussed in Chapter 7, over-end withdrawal is used to pull the yarn off the ring spinning bobbin in the direction of the bobbin axis, and the yarn passes through a pigtail guide on the axis. At withdrawal speeds of up to, say 25 m/min, the yarn tends to follow a direct path from the unwinding point on the package to the guide. In this situation, the yarn tension is almost entirely the result of frictional drag on the package surface. Winding speeds are very much higher than 25 m/min. At these higher speeds, the yarn balloons and, similar to ring spinning, the balloon geometry is determined by the equilibrium of the above-mentioned forces.

Yarn ballooning is a physical phenomenon of practical interest. It sets the minimum distance of separation that must occur between spindle positions on a ring-spinning machine so as to prevent adjacent balloons from colliding. Stable ballooning is essential for reduced machine stoppages. Balloon stability governs the balloon height/ring diameter relationship and thereby the package size. These factors, in turn, influence the production rate, energy cost, and (in certain cases) fabric quality.

In this chapter, we consider the main physical factors that determine yarn tensions and balloon geometry in ring spinning and winding. The study of yarn balloons was first reported in the literature in 1883 by Escher.[1] Since then, various other studies have been published; some qualitative, others mathematical, several involving fairly complex mathematics employing numerical methods and computer software to obtain exact predictions. Several investigators, however, have made simplifying assumptions to circumvent the mathematical difficulties of the more rigorous approach. Although analyses based on simplifying assumptions give less exact solutions, they are nevertheless useful for gaining a general understanding of the physics of yarn balloons. The justification for this is that such treatments are

easier to understand, yet they readily explain the essential physical phenomena involved and generally lead to results that are in good agreement with observations. Importantly, the results obtained were found to be a useful practical guide for predicting balloon performance. Although reference is made to the more complex solutions, including a number of the latest reported models, the descriptions given in this chapter will therefore follow the semiquantitative approach of some of the reported work, based on simplified assumptions. In particular, it is assumed that the forces acting on the yarn are sufficiently large for the effect of yarn stiffness to be negligible. Also, we assume that the yarn tensions do not cause any appreciable yarn extension. The yarn therefore can be viewed as an inextensible string.

8.1.1 Circularly Polarized Standing Waves

Consider a rotating string as shown in Figure 8.1.[17] The sideways appearance would be similar to that of the string vibrating in the vertical plane to form a standing wave or stationary wave.[2] In the case of the rotating string, we can refer to the waveform as a *circularly polarized standing wave.* Depending on the length, frequency of rotation, and tension of the string, there may be one or more nodal points.

In spinning and winding, yarn balloons are essentially circularly polarized transverse vibrations of a string. Thus, we can apply the basic equations for the velocity, c, of propagation of transverse waves along a string.

$$c = \left[\frac{T_a}{m}\right]^{\frac{1}{2}} \tag{8.1}$$

and

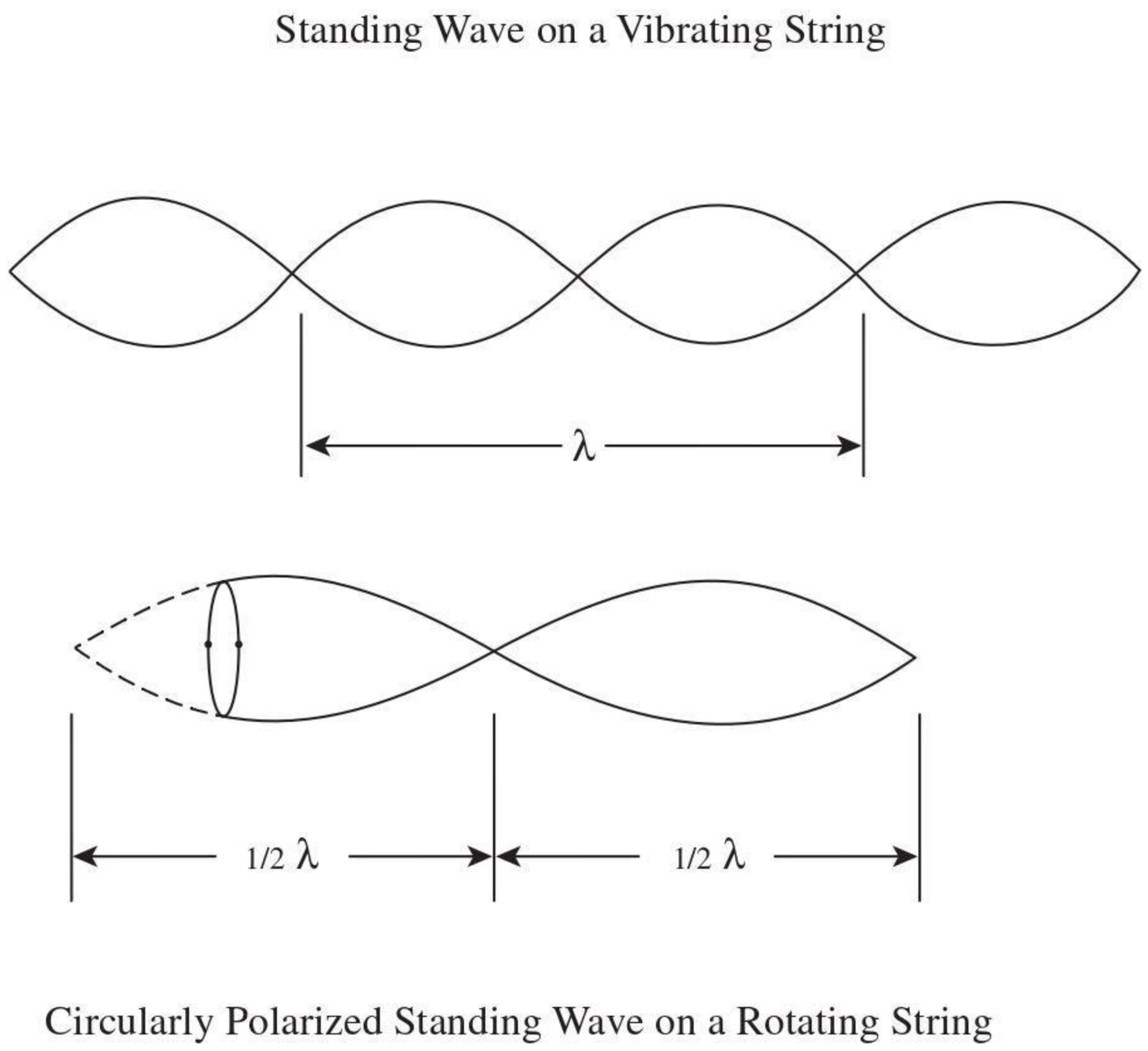

FIGURE 8.1 Circularly polarized standing waves.

$$\lambda = \frac{c}{f} \tag{8.2}$$

where T_a = tension in the string
m = mass per unit length
λ = wavelength
f = vibration frequency

The tension in the string is an important factor in balloon dynamics, and we will therefore first consider how tension arises in the yarn during ring spinning, followed by the balloon dynamics of this spinning system, and then extend the discussion to the winding process.

8.2 YARN TENSIONS IN RING SPINNING

In ring spinning, tension develops in the yarn mainly because, to move the traveler and the balloon length, L_b, around the common axis, and to wind the yarn onto the spinning bobbin, work must be done against the frictional force of the ring on the traveler and of the traveler on the yarn, as well as against the air drag on the traveler and on the balloon length. This work is additional to that needed to overcome the friction of the spindle bearings and the air drag on the forming yarn package.

The tensions in the yarn during ring spinning may be considered with respect to three zones: the winding zone, the balloon zone, and the yarn formation zone. The winding zone is the area in which the yarn length from traveler to forming package develops a winding tension, T_w. In the balloon zone, tension occurs in the yarn length between the traveler and lappet guide (often referred to as the *balloon tension*). This tension, at a given point on the balloon length, varies with amplitude (i.e., the radius of the point) measured from the common axis. At the ring and traveler, the balloon tension is provided by T_R and is related to T_w by Equation 6.6, given in Chapter 6.

In the yarn formation zone (i.e., the zone between the pigtail lappet guide and the front rollers of the drafting system), the yarn tension is termed the *spinning tension,* T_S, and is related to the balloon tension at the lappet guide, T_O, by Equation 6.5 in Chapter 6. To avoid confusion with symbols used later in this chapter, Equations 6.5 and 6.6 may be rewritten as

$$T_S = T_O\, e^{-\eta\theta} \tag{8.3}$$

$$T_R = T_W\, e^{-\upsilon\alpha} \tag{8.4}$$

To understand the physical causes of these tensions in the yarn, we need to consider the forces acting on the yarn in the three zones.

8.2.1 YARN FORMATION ZONE

Although the yarn rotates around the inner circumference of the lappet guide at almost the same speed as the traveler, the radius of the lappet guide is sufficiently

small for any central forces generated to be ignored. The motion of the yarn between the lappet and front drafting rollers is therefore principally related to the velocity along its length (i.e., the thread line velocity). Consequently, the forces of interest are the air drag along its length, the tension at the lappet guide, and the resistance to bending around the guide. The air drag is proportional to the square of the thread line velocity, but this velocity is usually small as compared with the rotational velocity of the yarn. Thus, the force caused by the air drag along the yarn length is assumed to be negligible. The bending resistance due to the flexural rigidity of the yarn is many times smaller than T_O and can also be omitted from further consideration. T_O is therefore the only effective force governing T_S and, as a result, analysis of the forces present in ring spinning is usually concerned with the remaining two zones.

8.2.2 Winding Zone

In steady running conditions, the traveler presses against the bottom of the internal flange of the ring, as illustrated in Figure 8.2.[17] The forces acting on the traveler at the point of contact with the ring are also depicted.

Strictly, T_W is not the true winding tension. This is because centripetal, Coriolis, and air-drag forces act on the mass of the yarn length from the traveler to the ring bobbin. It can be reasoned that the latter two effects negate each other and therefore can be neglected. The effect of the centripetal force is to change the path of the yarn from that of a tangent from the package to the traveler, to one of a curve. The change, however, is small and, for the sake of simplicity, this centripetal force is also neglected.

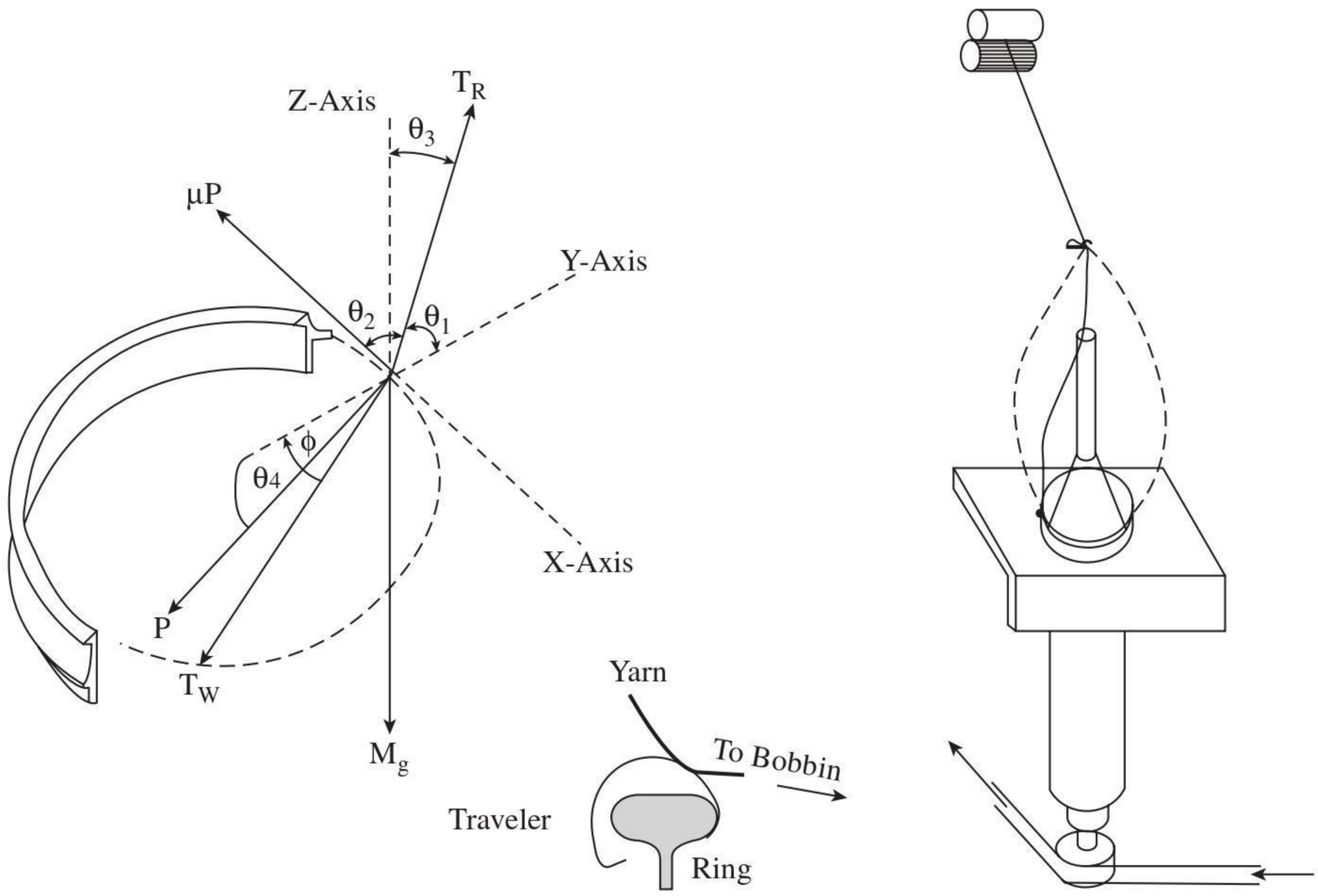

FIGURE 8.2 Forces acting on traveler during steady running conditions.

The simplified approach to relating the tensions of Equations 8.3 and 8.4 to the physical parameters of spinning is to first consider the forces acting on the yarn in the absence of air drag and then to introduce the effects of the drag component.

8.2.2.1 Yarn Tensions in the Absence of Air Drag

Let us first consider tensions T_R and T_W and the other forces acting on the traveler during steady running conditions (i.e., dynamic equilibrium). Resolving the forces shown in Figure 8.2 into their vertical and horizontal components gives

$$C = T_W \cos\phi + P \cos\theta_4 - T_R \cos\theta_1 \tag{8.5}$$

$$T_W \sin\phi = \mu P + T_R \cos\theta_2 \tag{8.6}$$

$$T_R \cos\theta_3 = P \sin\theta_4 + Mg \tag{8.7}$$

where $\theta_1 \ldots \theta_4$ and ϕ = angles indicated

C = centripetal force $\{MR\omega^2\}$ needed to keep the traveler circulating around the ring

P = reaction force of the ring and traveler

R = ring radius

Mg = weight of the traveler

μ = friction coefficient between ring and traveler

From Equations 8.4, 8.5, and 8.6,

$$T_R = \chi\mu\ C/\{\sin\phi \cos\theta_4 + \mu\cos\phi - \chi\ [\mu \cos\theta_1 + \cos\theta_4 \cos\theta_2]\} \tag{8.8}$$

and

$$\chi = e^{-\upsilon\alpha}$$

Equations 8.4, 8.6, and 8.7 give

$$\sin\theta_4 = \frac{\chi\mu[T_R\cos\theta_3 - Mg]}{T_R[\sin\phi - \chi\cos\theta_2]} \tag{8.9}$$

To simply the above equations and obtain an estimate for T_R, we can assume that the weight of the traveler, Mg, is negligible in comparison to T_R so that Mg can be removed from the equations. From practical observation, it is also reasonable to assume that θ_3 is such that $\cos\theta_3 = 1$. In the absence of air-drag, $\theta_2 \rightarrow 90°$, so $\cos\theta_2 \rightarrow 0$ (with $\rightarrow$ indicating "approximates to"). Hence, $\cos\theta_1 \rightarrow 0$, and $\chi\ \mu \cos\theta_1$ can be removed the equations. Based on these assumptions, Equations 8.8 and 8.9 become

$$T_R = \chi\mu\ C/\{\sin\phi \cos\theta_4 + \mu \cos\phi\} \tag{8.10}$$

$$\sin\theta_4 = \frac{\chi\mu}{\sin\phi} \tag{8.11}$$

From 8.11, $\cos\theta_4 = [\sin^2\phi - (\chi\mu)^2]^{1/2}/\sin\phi$. Equation 8.10 then becomes

$$T_R = \frac{\chi\mu C}{\{[\sin^2\phi - (\chi\mu)^2]^{1/2} + \mu\cos\phi\}} \tag{8.12}$$

From deriving T_R, we can now determine the winding tension from Equations 8.4 and 8.12.

$$T_W = \frac{\mu C}{\{[\sin^2\phi - (\chi\mu)^2]^{1/2} + \mu\cos\phi\}} \tag{8.13}$$

From the above equation, we can deduce certain important general information about the ring spinning system. Equations 8.6, 8.12, and 8.13 show that the yarn tensions T_R and T_W and the frictional drag of the ring on the traveler (μP) are directly proportional to the mass of the traveler, the ring diameter, and the traveler speed or spindle speed.

It can be seen from Equations 8.12 and 8.13 that, when μ is small, such that $\sin\theta_4 \to 0$, and $\cos\theta_4 \to 1$, then $T_R \to \chi\mu C/\sin\phi$ and $T_W \to \mu C/\sin\phi$. We can see, too, that frictional drag of the ring on the traveler is dependent on ϕ; $\mu P = T_W \sin\phi$. In general, then, as the package builds up, the winding tension will decrease with the lead angle ϕ determined by the frictional drag of the ring on the traveler, and also of the traveler on the yarn, as the latter passes through the former to the package. During a typical bobbin build, $\sin\phi$ can vary from between 0.45 and 0.5 (empty) to between 0.9 and 0.95 (full), so T_W can almost halve in size during the package build. The variation of T_W during the package build will therefore give a nonuniform package hardness, decreasing in hardness from the inside to outer layers. With a given ring diameter, this governs the amount of yarn that can be wound onto a bobbin.

For a fixed spindle speed and ring diameter, altering the traveler friction and mass will provide a particular winding tension, say, for a package of required hardness. For example, if μ is small, a heavier traveler will be needed than when μ is large. If μ is fixed, the tension becomes governed by the traveler mass. Thus, the selection of the traveler will depend on the maximum tension that the yarn will withstand when winding on an empty bobbin.

Figure 8.3 shows two possible running positions for the traveler. The normal running position is of the traveler contacting the inside of the ring. However, if too light a traveler is used, $T_W \cos\theta_4$ becomes greater than the centripetal force, C, and the traveler runs on the outside of the ring; this is termed *outside tracking*.

Consider now Equation 8.10. With regular running, $\theta_4 < 90°$ and $\cos\theta_4$ is positive. With outside tracking, $\theta_4 > 90°$ and $\cos\theta_4$ is negative. However, T_R and T_W would still be positive, and spinning would still occur if $\mu\cos\phi > \sin\phi\cos\theta_4$. This means that, at low winding angles, a minimum μ is necessary: $\mu > \tan\phi\cos\theta_4$ or, substituting for $\cos\theta_4$, $\mu > \sin\phi/[(\chi^2 + \cos^2\phi]^{1/2}$. The mean winding tension, T_W, is greater for outside tracking than for regular running, and abnormally high tension fluctuations occur, making the situation unstable.

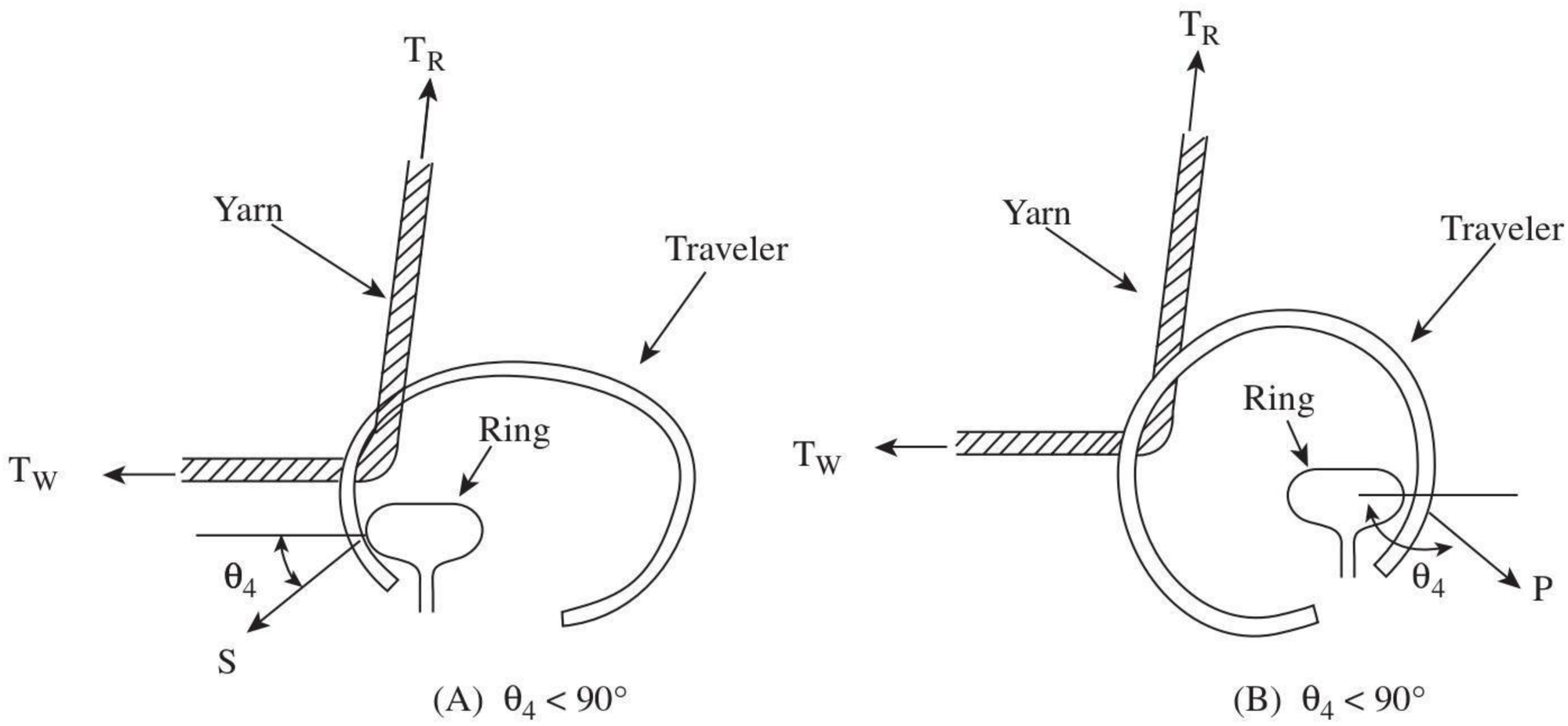

FIGURE 8.3 Normal running and outside tracking of traveler.

The coefficient of friction, μ, is speed dependent, decreasing with increasing speed. Outside tracking can therefore occur at low spindle speeds. Figure 8.4[17] illustrates the condition for outside tracking for a traveler mass of 40.3 mg.[8] The figure shows how winding tension, T_W, varies with μ and ν. The dotted parts of the curves indicate the conditions for outside tracking. The curve υ = 0.5 shows that there is also a limiting value of μ below which spinning cannot occur. This situation can be reasoned from Equation 8.11. Since $\sin\theta_4$ cannot be greater than unity, there must be a minimum value of ϕ, for a given μ and χ, below which the traveler will

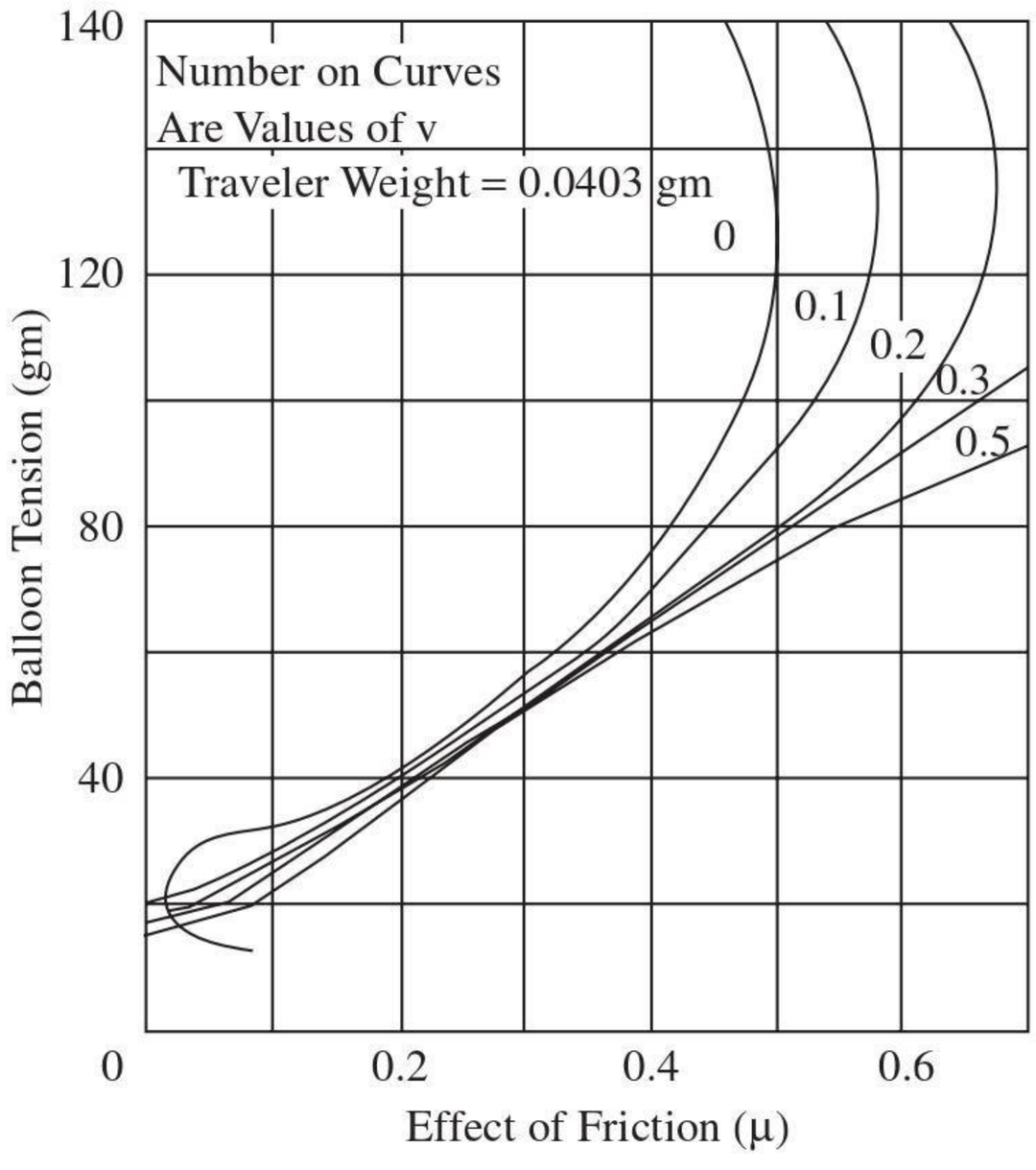

FIGURE 8.4 Relation between balloon tension, $T_{R,}$ and friction coefficients, P and μ.

not operate. This is given by $\sin\phi = \mu\chi$. The situation is readily seen if attempts are made to spin on empty bobbins of too small a diameter in relation to the ring diameter. This gives too small a ϕ value for the traveler to run. As wide as possible a winding angle is always beneficial and, as a general rule of thumb, the practice is for the empty bobbin to be at least half the ring diameter.

8.2.3 Balloon Zone

Let Figure 8.5 represent the balloon length in three-dimensional space as described in Chapter 6. Point o is the first nodal point of the balloon, and the origin of the axes z, x, y, which rotates with the spindle; z is essentially the spindle axis, and x = R is the ring radius.

To gain an understanding of the causes of tension in the balloon zone, we have to consider the forces acting on each elemental length, where r denotes the distance of an element of length from the z-axis. The forces present are as follows:

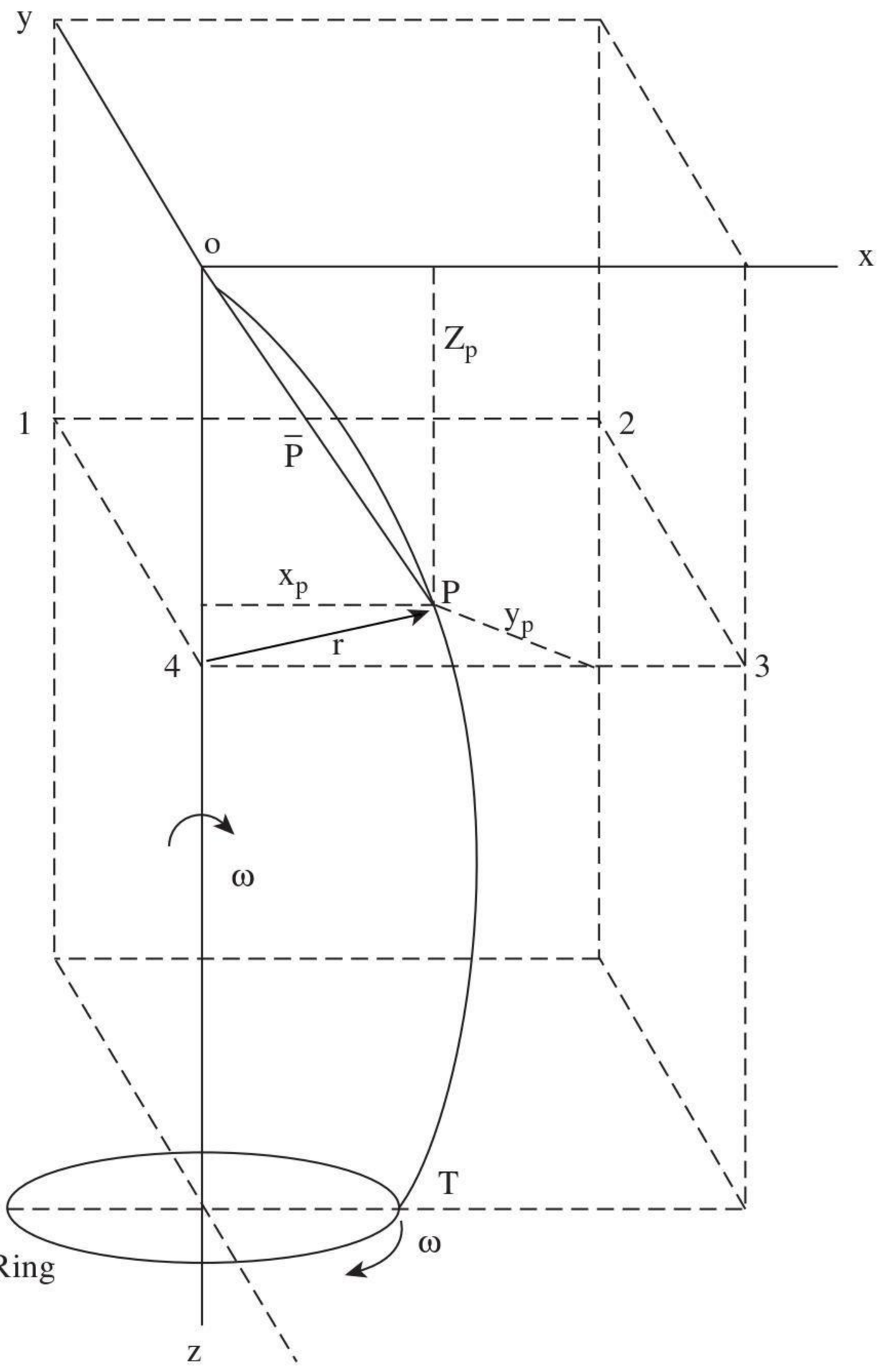

FIGURE 8.5 Three-dimensional representation of balloon length.

- Centripetal and Coriolis forces associated with the yarn motion
- Air drag forces opposing the yarn motion
- The weight of the element acting vertically downward
- The resistance to bending resulting from the flexural rigidity of the element

Let us look at these forces in a little more detail.

There are two components of centripetal force to consider. As an element, *dl*, of yarn moves from the lappet to the ring and traveler, a component of centripetal force acts on it to make it move through the curved path of the tread line. The size of this component of centripetal force mainly depends on the thread line velocity and is therefore considered to be negligible. The second component of centripetal force acting on the element keeps it rotating around the z-axis. As the angular velocity is high, this component is highly significant.

There are also two components of Coriolis force to consider. As the element of yarn rotates, it actually spirals from one radius to another due to the velocity of the yarn along its length, which gives the production speed. This velocity has three components: a radial velocity, a velocity tangential to the circumference of rotation, and a vertical velocity in the direction toward the ring and traveler. When moving from a smaller to a larger radius, the element's kinetic energy of rotation increases ($KE = 1/2\ mdlr^2\omega^2$) and decreases if the converse. The force acting on the element to cause the increase in KE is the component of Coriolis force associated with the radial velocity.

When KE increases, this component of force is in the direction of rotation but acts in the opposing direction for decreases in energy. Thus, as the element moves from the lappet guide toward the maximum balloon radius, assuming that this is greater than the ring radius, *R*, this component of force is in the same direction of rotation as the element. It is in the opposite direction when the element moves from the maximum radius to *R*. A second component of Coriolis force acts radially inward and is associated with the tangential velocity moving in the direction of rotation. These forces are of magnitudes $2mv_r\,\omega$ and $2mv_t\omega$, where v_r and v_t are the radial and tangential components of the thread line velocity. In ring spinning, because the thread line velocity is usually small by comparison with the rotational velocities, the two components of Coriolis force are neglected.

Similar to the above, there are two components of the air drag force present: the drag along the yarn length, which can be discounted for the reason given earlier, and the resistance of the air to the rotation of the element. The latter drag force component is regarded as being proportional to the square of the rotational velocity of the element relative to the air ($V_N^2 = [r\omega]^2$), which makes it important. This relation is probably not exact, since the power appears to be 1.7 as reported by WIRA.[3] However, the square law assumption is generally taken as a reasonable approximation. The velocity concerned is the component normal to the yarn surface. Hence, the air-drag force per unit length can be written as

$$A_D = 1/2\ \rho_A \xi d\ V_N^2 \tag{8.14}$$

where ρ_A = density of air

ξ = drag coefficient
d = yarn diameter
V_N = normal velocity component of the element dl as it passes through the air

Drag coefficient ξ is a function of the relative velocity, yarn diameter, and the kinematic viscosity of the air. However, in many calculated approximations for A_D, ξ is assumed to be constant. Yarn diameter d is the diameter of a smooth cylinder with equivalent air drag. This may be termed the *effective diameter.* Mack and Smart[4] found that, because of yarn hairiness, d varied with balloon speed. However, for the widest range of speeds, d did not greatly differ from the microscopic measured value.

The remaining two forces, *weight of element* and *resistance to bending,* may be assumed negligible in comparison with the other forces present.

8.2.3.1 Balloon Tension in the Absence of Air Drag

Since the balloon tension changes from one given point in the balloon length to another, to obtain an equation for the balloon tension at a point, we consider the forces acting on any element of the yarn balloon in the absence of air drag (see Figure 8.6[17]). The figure shows that, in this situation, the curve of the balloon length is in the x–z plane. Since the yarn axis lies within this plane, we can call it the *axial plane*.

Let dl be the element of length under consideration. If m is the mass per unit length of the yarn, then forces acting will be the centripetal force, $C = mdlx\omega^2$; the tension at both ends of dl, T, and $T + \Delta T$; the weight of the element acting vertically downward, $w = mdlg$; and the Coriolis force.

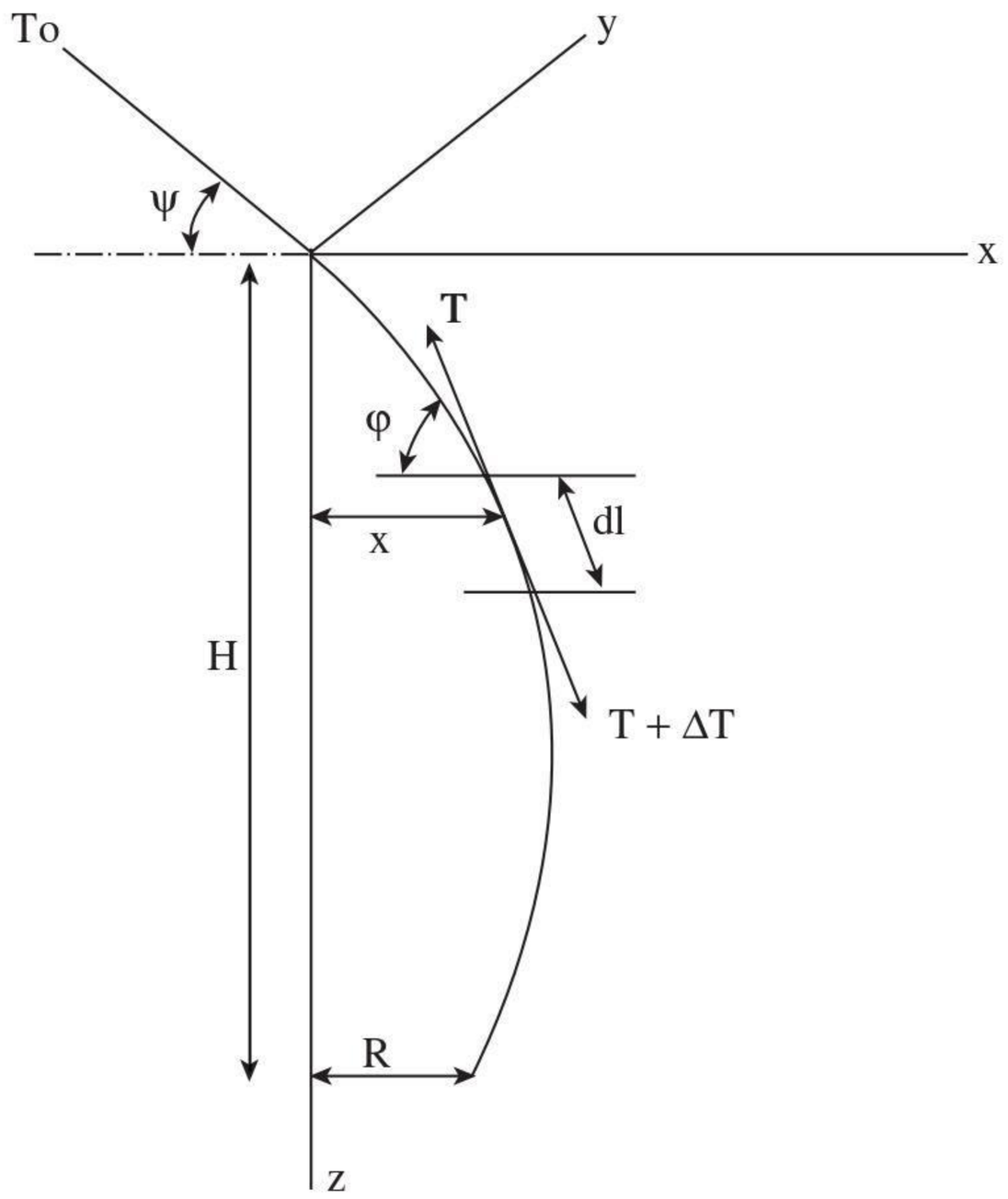

FIGURE 8.6 Yarn balloon in the absence of air drag.

In ring spinning, the rotational velocities are much higher than the velocity of the yarn along the thread line, so the Coriolis force can be neglected. It can also be assumed that the weight of the element is negligible as compared with the other forces present. For steady balloon shape, we can equate the resolved components of the remaining forces.

$$[T \sin\varphi + d(T \sin\varphi)] - T \sin\varphi = 0$$

or

$$d(T \sin\varphi) = 0 \tag{8.15}$$

$$T \cos\varphi - [T \cos\varphi + d(T \cos\varphi)] = mdlx\omega^2$$

or

$$d(T \cos\varphi) = -mdlx\omega^2 \tag{8.16}$$

Also,

$$\cos\varphi = \frac{dx}{dl} \tag{8.17}$$

Using $\frac{d(UV)}{d\varphi} = V\frac{dV}{d\varphi} + U\frac{dV}{d\varphi}$ and $\frac{d}{dl} = \frac{d\varphi}{dl} \cdot \frac{d}{d\varphi}$, the equations become

$$\sin\varphi\frac{dT}{d\varphi} + T\cos\varphi = 0$$

i.e.,

$$d\varphi/\tan\varphi = -dT/T \tag{8.18}$$

and

$$\cos\varphi\frac{dT}{dl} - T\sin\varphi\frac{d\varphi}{dl} = -mx\omega^2$$

$$T \sin\varphi\, d\varphi - \cos\varphi\, dT = mdlx\omega^2 \tag{8.19}$$

From Equation 8.18, substituting for $d\varphi$ in 8.19,

$$-dT/\cos\varphi = mdlx\omega^2$$

and from Equation 8.17,

$$-dT = m\ \omega^2\ x\ dx$$

Integrating, we get

$$T = T_O - \frac{1}{2} mx^2\omega^2 \tag{8.20}$$

Integrating Equation 8.18,

$$\log \sin \varphi + \text{constant} = -\log T + \text{constant, or}$$

$$\sin \varphi / \sin \varphi_0 = \frac{T_O}{T} \tag{8.21}$$

where φ_0 = the angle of yarn element just below the lappet guide

Equations 8.20 and 8.21 describe the tension variation along the balloon length in the absence of air drag. The tension is a maximum at the thread guide and a minimum at the maximum balloon radius. It should be noted that the high tension at the guide is a disadvantage, because it restricts the twist propagation to the front rollers of the drafting system. The yarn length from the guide to the front rollers is therefore susceptible to peak tension fluctuations, particularly if the mean value of T_O, and thereby T_S, is high.

8.2.3.2 Spinning Tension in the Absence of Air Drag

We see from Figure 8.6 that, in basic ring spinning, the balloon shape is approximately half a cycle, i.e., $H = 1/2\ \lambda$. Referring to Equations 8.1 and 8.2, $T_a = T_O$ (in units of newtons), the tension in the yarn balloon at the lappet guide, m, is mass per unit length (in units of kg/m), $f = N_t$ (in units of s^{-1}).

Thus, T_O can be obtained from rearranging the equations to give

$$\frac{1}{2}\lambda = \pi\ P \tag{8.22}$$

where

$$P = [T_O / \omega^2 m]^{\frac{1}{2}} \tag{8.23}$$

and

$$\omega = 2\ \pi N_t \tag{8.24}$$

Hence,

$$H = \pi\ P \tag{8.25}$$

Equation 8.23 can be rewritten in terms of yarn count, T_t, in tex to give

$$P = K\left[\frac{T_O}{N_t^2 T_t}\right]^{\frac{1}{2}}$$

where K is an appropriate constant. Knowing T_O, the spinning tension, T_S can be found from Equation 8.3.

Figure 8.6 and Equation 8.20 show that, when $x = R$,

$$T_R = T_O - \frac{1}{2} mR^2\omega^2 \tag{8.26}$$

Hence, Equations 8.12 and 8.26 give

$$T_O = \frac{\chi\mu C}{\left\{[(\sin^2\phi - (\chi\mu)^2)]^{\frac{1}{2}} + \mu\cos\phi\right\}} + \frac{1}{2}mR^2\omega^2 \tag{8.27}$$

This equation shows how T_O, and thereby T_S, is also dependent on the winding angle, the traveler mass and angular velocity, and the coefficients of friction of the ring and traveler and the yarn and traveler.

Figure 8.7 depicts how, theoretically, the ratio $T_R/C \cong T_O/C$ varies with ϕ, μ, and χ.[17] It is evident that all the tensions decrease similarly with these parameters. The dashed curve depicts the deviation of experimental values, which is attributed to the effect of air drag neglected in the analysis.

8.2.4 The Effect of Air Drag on Yarn Tensions

In the absence of air drag, the balloon length lies in the x–z plane, i.e., the vertical or axial plane. With the presence of air drag, the yarn becomes inclined to the axial plane in such a way that, moving from the lappet guide to the ring, each succeeding element of length is more inclined. We therefore have to consider the balloon length in three-dimensional space as shown in Figure 8.5, where r instead of x now denotes the distance of each element of length from the z-axis.

A rigorous analysis of the effect of air drag on the yarn tensions involves determining how the angles θ_1 through θ_4 in Figure 8.2 vary as ϕ changes during winding. This involves complex mathematics, which may be circumvented by a very simplified approach.[2]

We saw that, in the absence of air drag, there was effectively only a vertical component of tension in the balloon length, which corresponded to the winding tension needed to overcome the ring-traveler friction. Since air drag inclines the balloon length, its effect is to introduce a horizontal component of tension, causing a corresponding increase in the winding tension. Essentially, then, we can assume that the presence of air drag introduces a tension component in the balloon length, which is added to the frictional drag of ring on traveler to resist the traveler motion. If D is this added resisting force, Equation 8.8 can be modified to give

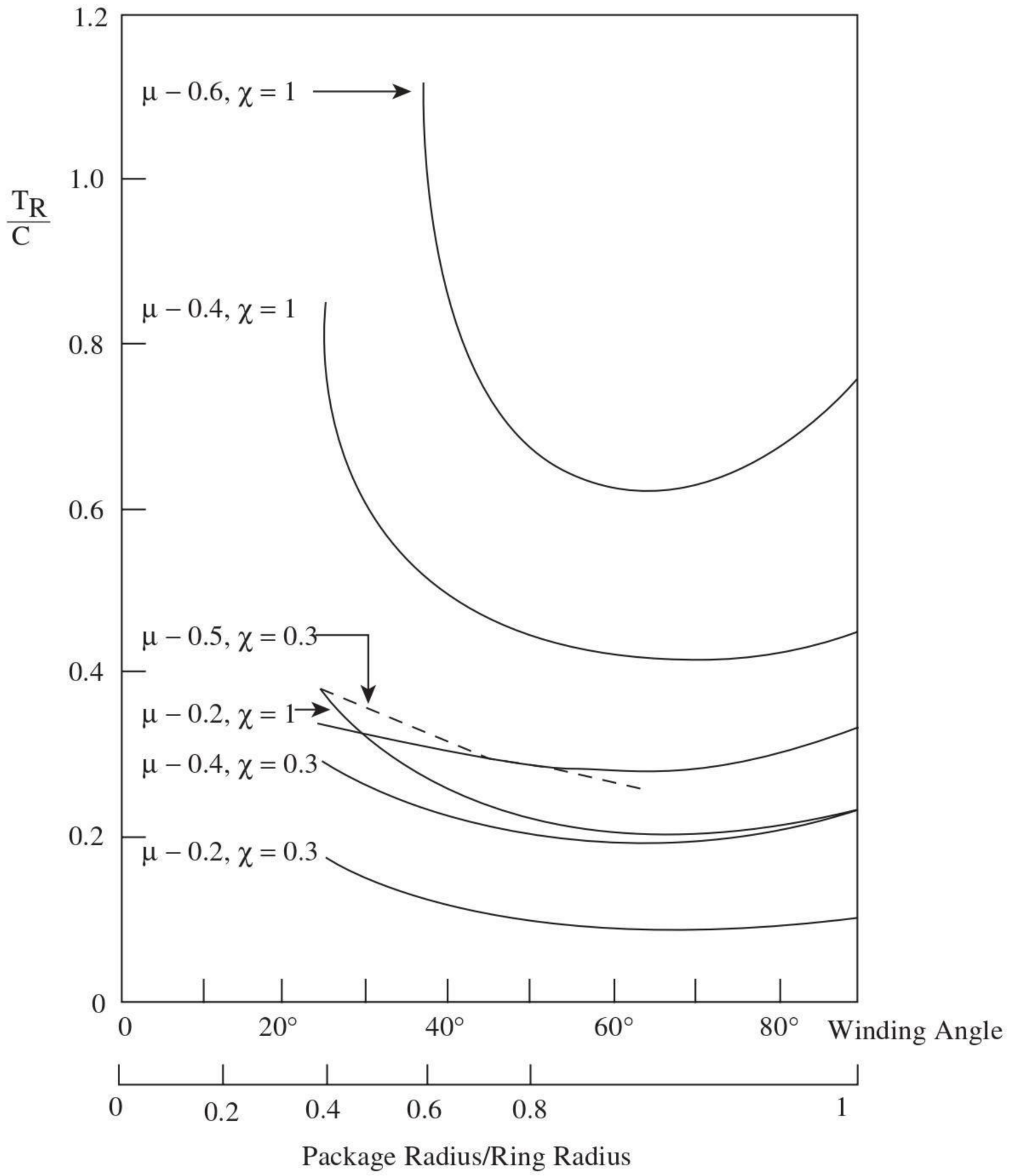

FIGURE 8.7 Yarn tension as a function of winding angle ϕ and friction coefficients.

$$T_R = \frac{\chi(\mu C + D\cos\theta_4)}{\{\sin\phi\cos\theta_4 + \mu\cos\phi - \chi[\mu\cos\theta_1 + \cos\theta_4\cos\theta_2]\}} \tag{8.28}$$

To derive D, we to consider the tension components in an element of balloon length dl at distance r (see Figure 8.8). The air-drag force is given by Equation 8.14 and, from Figure 8.8, $V_N = r\omega\cos\alpha$.

The mechanical power to overcome the air drag on dl is

$$1/2\ \rho_A \xi d\ r^3\omega^3\ dl\ \cos^2\alpha$$

For the full balloon length, we integrate from 0 to L_b

$$1/2\ \rho_A \xi d\omega^3 \int_0^{Lb} r^3\cos^2\alpha\ dl$$

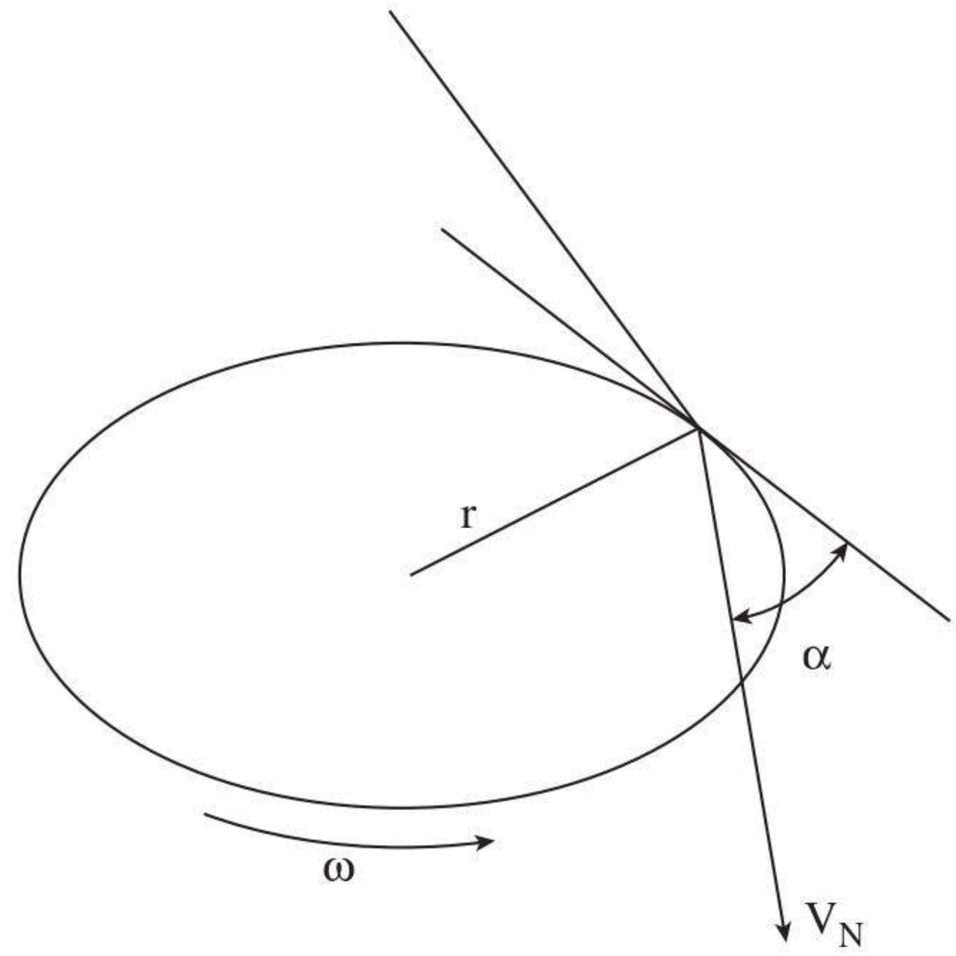

FIGURE 8.8 Relationship between air drag force and normal component of air velocity.

Now, if T_{RA} is the tension in the balloon length at the position of the ring, caused by air drag, the above expression will be equal to $T_{RA} \cos\theta_2 R\ \omega$. Thus,

$$T_{RA}\cos\theta_2 = \frac{\rho_A \xi d \omega^2}{2R} \int_0^{L_b} [r^3 \cos^2\alpha] dl \tag{8.29}$$

All the parameters of the integral depend on the balloon shape and therefore on T_{RA}. For a simplified solution to the integral, we may assume that the balloon is sinusoidal,[2] so $r = r_{max} \sin(2\pi z/\lambda)$, and also that the air-drag force acts in the horizontal plane, so $\alpha = 0$.

Using $dl^2 = dr^2 + dz^2$ and $H = \lambda/2$, then, substituting for dl and r, Equation 8.29 can be now be rewritten as

$$T_{RA}\cos\theta_2 = \frac{\rho_A \xi d \omega^2}{2R} \int_0^{L_b} \left[r_{max}^3 \sin^3(2\pi z/\lambda) 2H \left\{ 1 + \frac{4\pi^2 r_{max}^2}{\lambda^2} \cos^2(2\pi z/\lambda) \right\}^{1/2} (dz/\lambda) \right]$$

and on integrating,

$$T_{RA}\cos\theta_2 = \frac{\rho_A \xi d \omega^2 H r_{max}^3}{4R} = D \tag{8.30}$$

Assuming that $\theta_1 = 90°$ and $\theta_3 = 90 - \theta_2$, which closely approximates the practical situation, Equation 8.28 becomes

$$T_R = \cos\theta_2 = \frac{\chi(\mu C + D\cos\theta_4)}{\sin\phi\cos\theta_4 + \mu\cos\phi} = D \tag{8.31}$$

where D = as given by Equation 8.30

The yarn tensions, T_W, T_O, and T_S can be therefore calculated with Equations 8.3, 8.4, 8.26, and 8.28.

8.3 BALLOON PROFILES IN RING SPINNING

The importance of predicting the balloon shape from set parameters of the spinning geometry was explained at the start of this chapter. With respect to balloon dynamics, the important parameters of the spinning geometry are the balloon height, H, the ring radius, R, the spindle rotational speed (more correctly, the *traveler speed*), ω, and the spinning tension, which is largely governed by the traveler mass.

The objective is to choose these parameters so that we can obtain an acceptable spinning package size without incurring increased unit cost of production or reduced yarn quality. It is therefore useful to have some means of determining if certain combinations of the spinning geometry parameters will give a stable balloon (i.e., $H \approx 1/2\lambda$). One approach would be to theoretically derive a relationship where the radius, r, of any element of the ballooning yarn length is given as function of the distance, z, along the common axis from the origin, which is the lappet guide. For given spinning parameters, such an equation would enable graphs to be plotted of spinning balloons.

Mack[5] developed the set of differential Equations 8.32 to 8.35, given in Table 8.1, for the three-dimensional motion of an element, dl, of ballooning yarn length l, based on the forces discussed above acting on the element during spinning. The variables x, y, z refer to the Cartesian coordinates. Mack's equations do not account for movement along the thread line and so effectively assume the circulating balloon length to be a constant length between the lappet and the traveler. This may be called a *tied-balloon model.* A more recent model, proposed by Lisini et al.,[6] uses partial differential equations to take account of the effect of ring rail motion and variations in traveler speed. However, the simplifying assumptions that apply to the tied-balloon model facilitate an easier and more practical understanding of the spinning balloon.

These equations can only be solved directly by numerical integration, for example, using the Runge–Kutta method.[8,9] By carrying out the following multiplication and addition: $(8.32)(dx/dl) + (8.33)(dy/dl) + (8.34)(dz/dl)$, we get $dT/dl + m\omega^2 (xdx/dl + ydy/dl) = 0$, and this can be integrated to give $T = T_O - 1/2\ m\omega^2\ [x^2 + y^2]$. Using this and dividing x, y, and z by P from Equation 8.23, we get the nondimensional forms $X = x/P$, $Y = y/P$ and $Z = z/P$, $\lambda = KP/m$. Similarly, $L = l/P$ and $R = r/P$, where l refers to the balloon length and r the radius of any point on the balloon from the axis z. Thus, Equations 8.32 to 8.35 can be converted to the simpler form of Equations 8.36 to 8.38 using $X = R\cos\delta$ and $Y = R\sin\delta$, where δ is the angle of deviation of the balloon element from x–z plane. These equations enable analytical solutions to be made that can be used to make adequate predictions of balloon stability. The approach that is used is to first establish predicted balloon shapes or profiles in the absence of air drag and then to modify these for the presence of air drag.

TABLE 8.1
Differential Equations of Motion of a Ballooning Yarn Element[5]

$$\frac{d}{dl}(Tdx/dl) + mx\omega^2 + K\omega^2\{x^2 + y^2 - (x\ dy/dl - ydx/dl)^2\}^{1/2}$$
$$\left[y + \frac{dx}{dl}(xdy/dl) - ydx/\mathrm{dl}\right] = 0 \tag{8.32}$$

$$\frac{d}{dl}(Tdy/dl) + my\omega^2 + K\omega^2\{x^2 + y^2 - (x\ dy/dl - y\ dx/dl)^2\}^{1/2}$$
$$\left[-x + \frac{dy}{dl}(xdy/dl - ydx/dl)\right] = 0 \tag{8.33}$$

$$\frac{d}{dl}(Tdz/dl) + 0 + K\omega^2\{x^2 + y^2 - (x\ dy/dl - y\ dx/dl)^2\}^{1/2}$$
$$\left[\frac{dz}{dl}(xdy/dl - ydx/dl)\right] = 0 \tag{8.34}$$

$$(dx/dl)^2 + (dy/dl)^2 + (dz/dl)^2 = 1 \tag{8.35}$$

TABLE 8.2
Converted Equations of Motion of a Ballooning Yarn Element[5]

$$\frac{d}{dL}\{(1 - R^2/2)dR/dL\} + R - (1 - R^2/2)R(d\delta/dL)^2$$
$$+\lambda R^3\frac{dR}{dL}\cdot\frac{d\delta}{dL}\{1 - R^2(d\delta/dl)^2\}^{1/2} = 0 \tag{8.36}$$

$$\frac{d}{dL}\{(R^2 - R^4/2)d\delta/dL\} - \lambda R^3\{(1 - R^2)(d\delta/dL)^2\}^{3/2} = 0 \tag{8.37}$$

$$(dR/\mathrm{dL})^2 + R^2(d\delta/dL)^2 + (dz/dL)^2 = 1 \tag{8.38}$$

8.3.1 Balloon Profiles in the Absence of Air Drag

We saw that, when considering balloon tensions, for the situation of no air drag, the balloon length may be assumed to be within the axial plane (see Figure 8.6). The angle $\delta = 0$, $\lambda = 0$, and Equation 8.36 becomes

$$d/dL\ \{[1 - 1/2\ R^2]\ dR/dL\} + R = 0 \tag{8.39}$$

Using $d(UV)/dx = UdV/dx + VdU/dx$, we get

$$-R(dR/dL)^2 + (1 - \frac{1}{2}R^2)d^2R/dL^2 + R = 0 \tag{8.40}$$

Multiply Equation 8.40 by $(1 - \frac{1}{2}R^2)$ and, using the relationship

$$d^2R/dL^2 = \frac{1}{2}\frac{d(dR/dL)^2}{dR}$$

we can integrate Equation 8.40 with respect to R, and since $dR/dL = \sin\psi$ when $R = 0$ (where ψ is the angle of the tangent to the balloon at lappet guide), then

$$R^2 - R^4/4 + [1 - R^2/2]^2(dR/dL)^2 - \sin^2\psi = 0$$

or

$$\left(\frac{dR}{dL}\right)^2 = \frac{\sin^2\psi - R^2 + R^4/4}{[1 - R^2/2]^2} \tag{8.41}$$

When $\delta = 0$, Equation 8.38 gives

$$\left(\frac{dZ}{dL}\right)^2 = 1 - (dR/dL)^2 = \frac{\cos^2\psi}{[1 - R2/2]^2}$$

If the coordinates R and Z are used in preference to X and Z, then

$$R = 2\sin\frac{1}{2}\psi\sin\zeta$$

and

$$\frac{dZ}{d\zeta} = \frac{dZ}{dL}\frac{dL}{dR}\frac{dR}{d\zeta} = \frac{\cos\psi}{\cos\left(\frac{1}{2}\psi\right)\left[1 - \tan^2\left(\frac{1}{2}\psi\right)\sin^2\zeta\right]}$$

which, on integrating, in the usual notation for elliptic integrals, gives

$$Z\cos(\frac{1}{2}\psi) = \cos\psi\ \mathrm{F}\ \{\tan(\frac{1}{2}\psi),\ \zeta\} \tag{8.42}$$

For most situations, $\psi < 65°$, and an approximate solution to 8.42 for a plot of R against Z is of a sinusoidal wave,

$$R = 2 \sin(\frac{1}{2}\psi) \sin\{[Z \cos(\frac{1}{2}\psi)\, f(\psi)]/\cos\psi\} \tag{8.43}$$

where $f(\psi) = \frac{2}{\pi} F(\tan(\frac{1}{2}\psi), \frac{1}{2}\pi)$, for which values are given below.

ψ^o	0	5	10	15	20	25	30	35	40
$f(\psi)$	1.000	1.000	1.002	1.004	1.008	1.013	1.019	1.026	1.034
ψ^o	45	50	55	60	65	70	75	80	85
$f(\psi)$	1.048	1.062	1.081	1.104	1.134	1.175	1.234	1.325	1.501

The above solution is attributed by Mack,[5] and Figure 8.9[17] shows a set of balloon profiles obtained from this solution. Gregory and Smart[10] have confirmed the validity of the solution for the case of negligible air drag.

Various approximate solutions of the balloon equation have been reported, most of which circumvent dealing with the elliptic integral. We shall now consider several of these, as they help us to further understand the nature of spinning balloons.

Lindner[11] assumed spinning balloons, in the absence of air drag, to be long and narrow so that dl is not much greater than dz. Then, referring to Figure 8.6, $T \sin\varphi$ = constant = T_b, the tension at maximum balloon radius. Also, $d(T_b \cos\varphi) = m\omega^2 r\, dz$, and $\cos\varphi = dr/dz$. Thus, $d^2r/dz^2 = -m\omega^2 r/T_b$. This is a differential equation of simple harmonic motion that has the solution

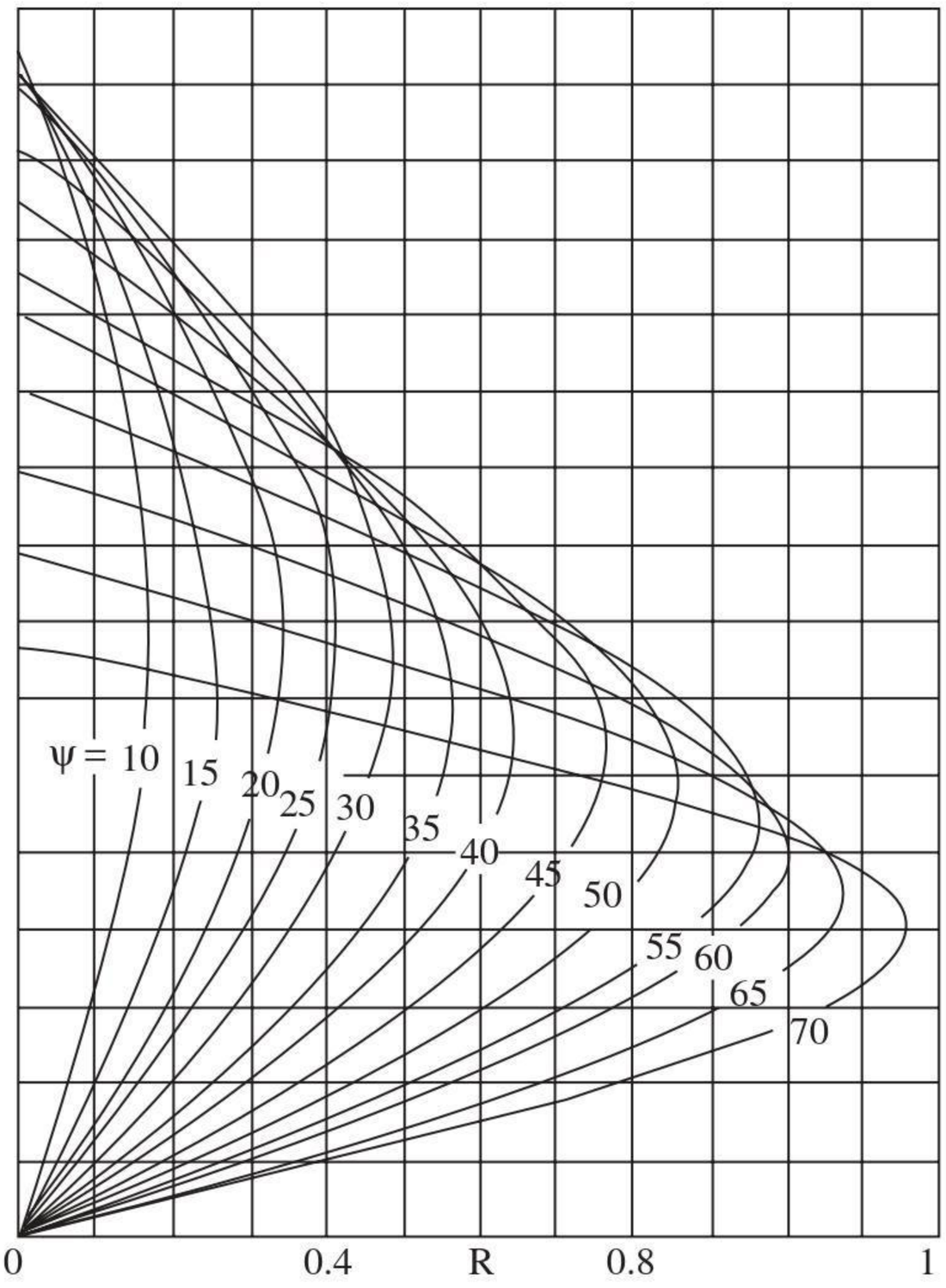

FIGURE 8.9 Balloon profiles based on Mack's solution.

$$r = A \sin\left[\left(\frac{m\omega^2}{T_b}\right)^{\frac{1}{2}} z\right] \tag{8.44}$$

This solution is also reported by Crank,[7–9] Grishim,[12] and Honneger and Fehr[13] and is claimed to give agreement with measurements of photographic images of balloons.

Bracewell and Greenhalgh[14] reported the case of long-lift, large-package spinning. They assumed that the associated balloons can be modeled by the Cartesian equation for a catenary. The result obtained was in good agreement with observations of balloon profiles for long-lift, large-package, ring-spinning systems.

De Barr[15] assumes balloon profiles to be sinusoidal and then develops the concept of the balloon profile being a standing wave system identical to circularly polarized, transverse vibrations of a string. De Barr's approach merits full consideration, as it is much less mathematical and gives comparable results to Mack's[5] more rigorous treatment.

First, the concept of circularly polarized, transverse vibrations should be further explained. When a string fixed at both ends is vibrated in, for example, the x–z plane, it will form a standing wave (a plane-polarized vibration) if its length equals an integral number of half-wavelengths. This is a classical experiment demonstrated by Melde in which one end of a string was attached to a vibrating tuning fork while the other was fixed. If the string is made to vibrate simultaneously with the same frequency in y–z plane, the string will move according to the resulting superposition of the two component vibrations. Thus, the movement of each point on the string will be the sum of two simple harmonic vibrations at right angles. If the amplitudes of the vibrations are equal and out of phase by 90°, then the motion of each point in the string will be circular about a central axis. We now have a circularly polarized standing wave instead of a plane-polarized one. The radius of the circle at points along the string, i.e., from the z-axis, will vary sinusoidally.

Since the idea is to use circularly polarized standing waves to represent the spinning balloon, Equations 8.1 and 8.2 can be used in relation to the balloon. An approximation of a balloon shape can be obtained once the amplitude and wavelength are known. For a given frequency, the speed of propagation, c, and thereby the wavelength, λ, of a vibrating string decrease with increased amplitude. De Barr applied Rayleigh's principle[16] (that the mean kinetic and potential energies of a vibrating system are equal) to obtain Figure 8.10,[17] showing the decrease in wavelength with increasing amplitude. Thus, for a range of arbitrary chosen λ values, various balloon profiles can be plotted from the following equation:

$$r = A \sin(2\pi z/\lambda)$$

or, nondimensionally,

$$r/P = A \sin(2\pi z/P\lambda) \tag{8.45}$$

where r = balloon radius
A = amplitude
z = distance along the common axis of spindle, ring, and spinning balloon

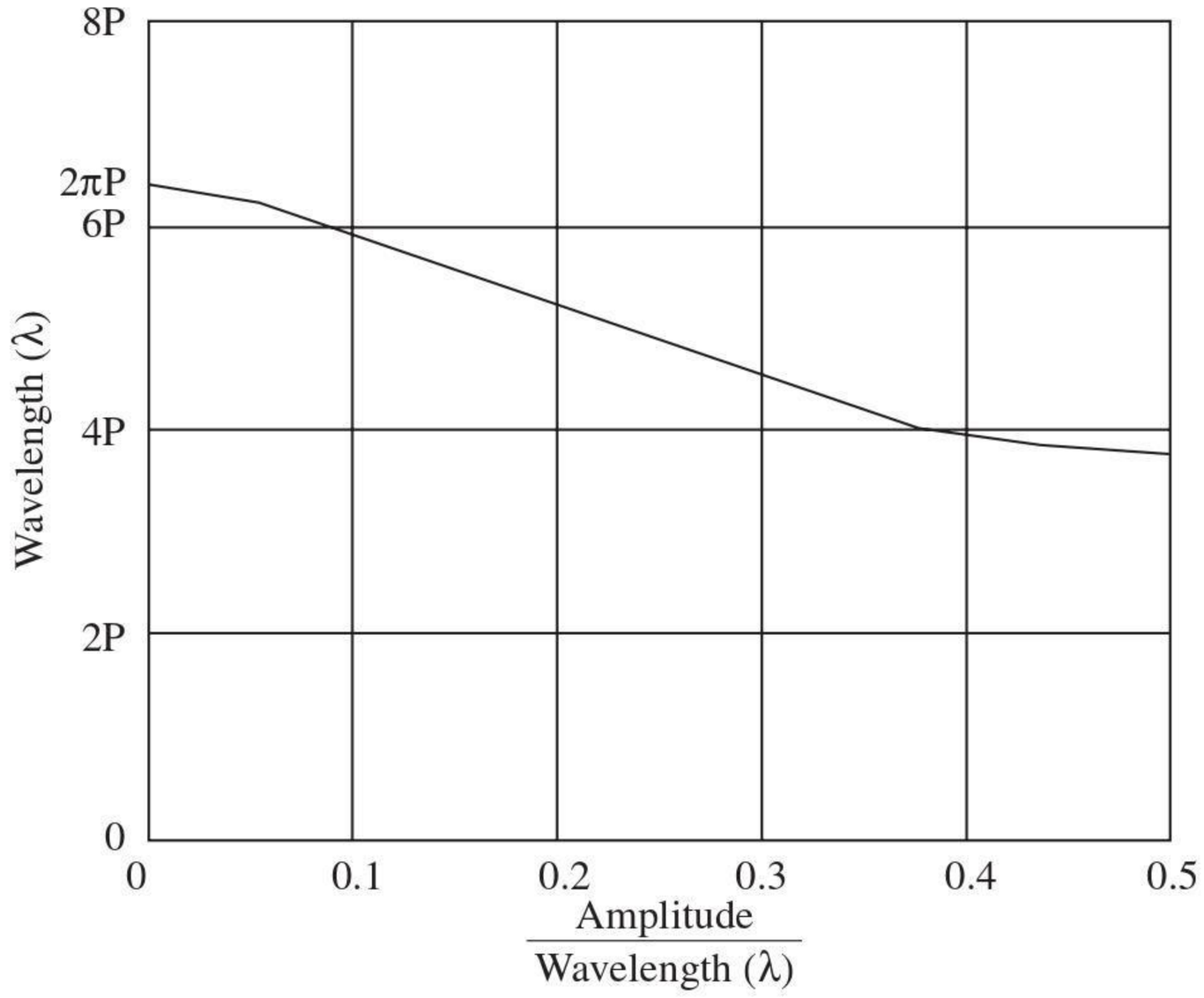

FIGURE 8.10 Decrease in wavelength with increasing amplitude.

An alternative approach is to use Equations 8.20 and 8.21. Noting that, in the absence of air drag, $r = x$, these equations can be combined to give

$$\sin\varphi\,(T_O - 1/2\; mr^2\omega^{2)} = T_O \sin\varphi_0 \tag{8.46}$$

Equation 8.46 gives the inclination of the balloon length at any radius and therefore enables the balloon shapes to be determined. At the maximum radius, $\varphi = 90°$ and hence, from Equations 8.21 and 8.46,

$$T = T_O \sin\varphi_0 \tag{8.47}$$

and

$$r^2_{max} = 2\,T_O\,(1 - \sin\varphi_0)/m\omega^2 \tag{8.48}$$

De Barr found that using Equations 8.46, 8. 47, and 8.48 gave balloon shapes similar to Mack's solutions. The balloon shapes calculated from these equations differ slightly from the sinewave Equation 8.45, as illustrated in Figure 8.11.[17] However, observations have shown that Equation 8.45 gives a better representation of actual balloons shapes, and this is attributed to effects of air drag.[15]

8.3.2 The Balloon Profile in the Presence of Air Drag

We must remember that the purpose of determining the balloon shape is to ascertain the spinning conditions that would result in balloon collapse, i.e., the tendency for a half-wavelength balloon profile to change to a profile with a second nodal point. If the balloon collapses onto the spindle, spinning cannot continue. Before describing

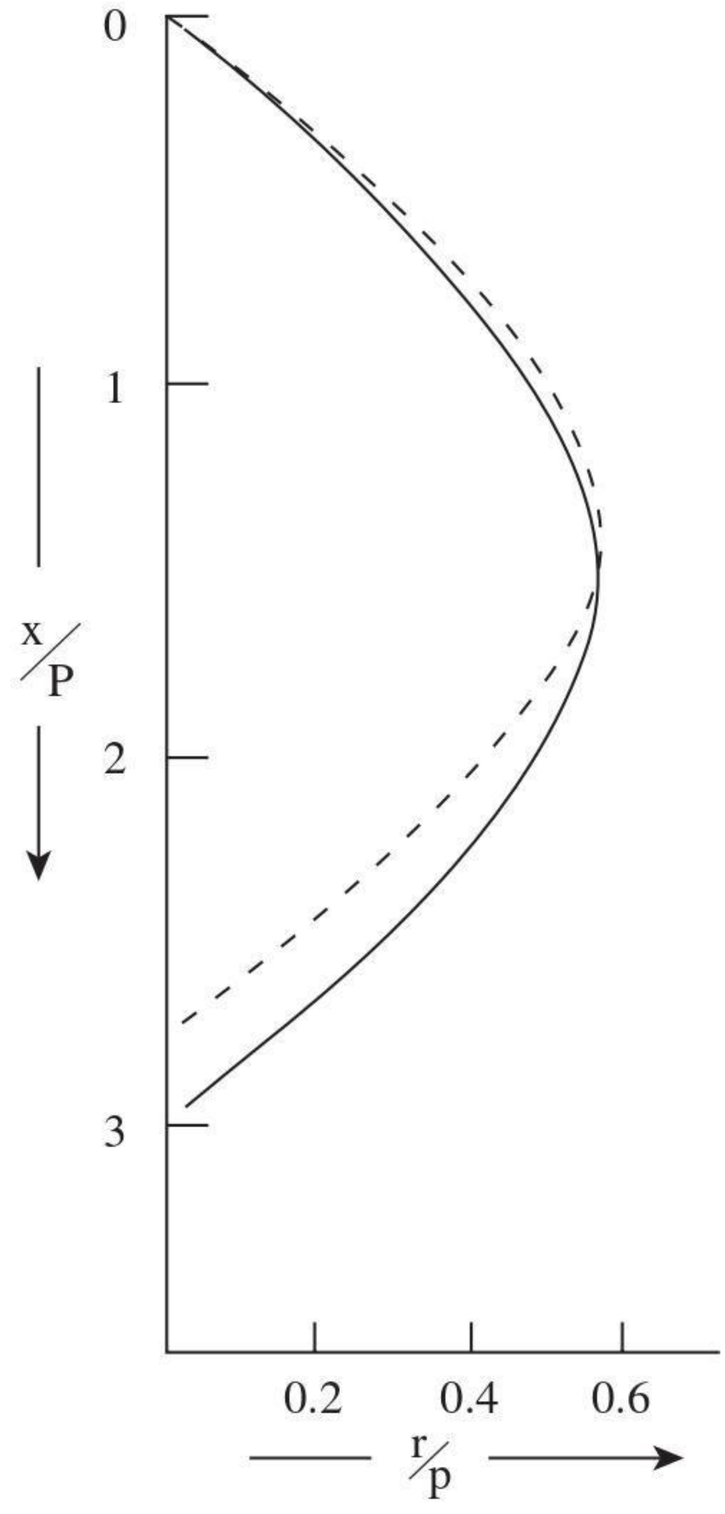

FIGURE 8.11 Decrease in wavelength with increasing amplitude.

how the optimal conditions to prevent balloon collapse can be ascertained from a graph of a series of balloon profiles, it is useful to address the effect of air drag on balloon profiles.

When simplifying the differential equations of balloon motion, given in Table 8.2, δ was referred to as the angle of deviation of a balloon element, *dl*, from the x–z plane. In discussing the effect of air drag on balloon tension, it was explained that the effect of the air was to introduce a tangential tension component in each yarn element. It is this tension that causes the angle of deviation. The component of tension is greater for yarn elements closer to the ring and traveler. Therefore, as Fig 8.12[17] illustrates, the angle of deviation, δ, of the balloon length increases toward the ring and traveler.[16]

Equation 8.14 shows that resistance of the air to the rotation of the balloon is proportional to the square of the normal component of yarn velocity relative to the air. However, if the tension in the yarn attributed to the ring and traveler is high, the tangential component induced by the air drag will be low, and δ will be small.

Dividing Equation 8.14 by *P/m* gives the nondimensional form for the air drag,

$$\gamma = mA_D/P = 1/2\ \rho_A \xi d\ mV_N^2/P \tag{8.49}$$

Figure 8.13 shows the projections onto the axial plane (i.e., z–x or z–r plane, when $x = r$) of several balloon profiles for various values of γ.[17] Comparing the

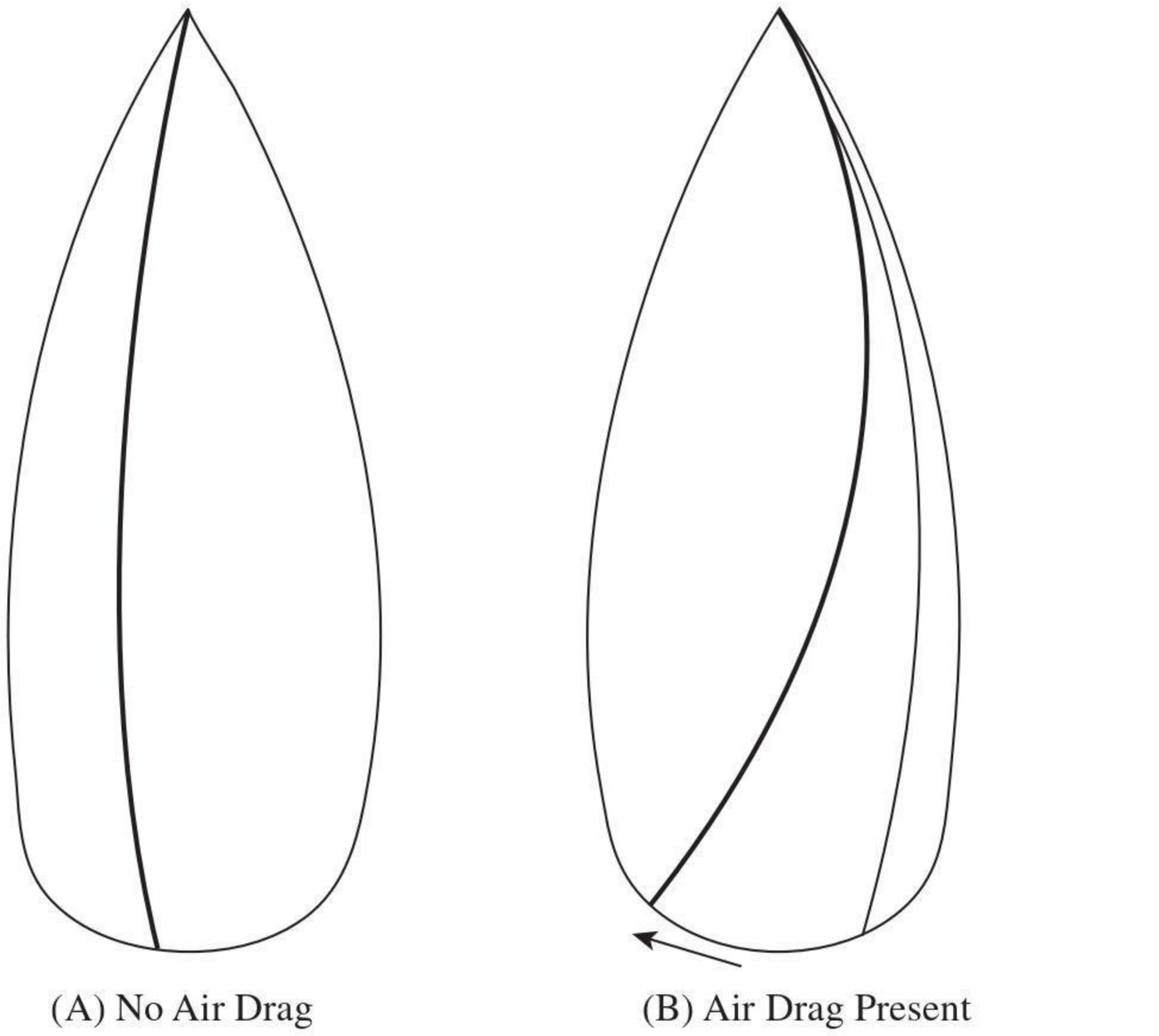

(A) No Air Drag (B) Air Drag Present

FIGURE 8.12 Shape of yarn balloon in absence of air-drag and the effect of air drag.

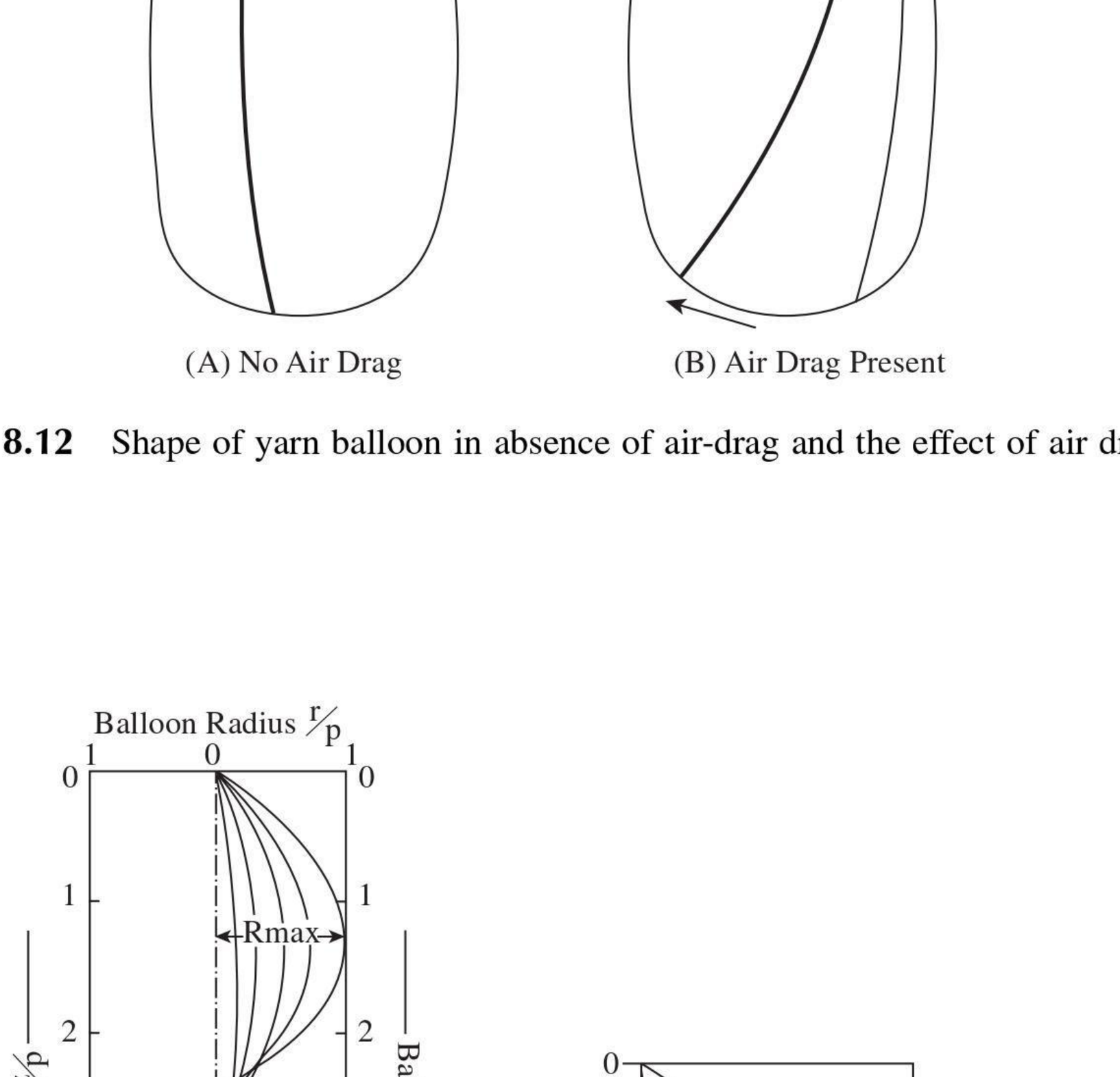

FIGURE 8.13 Projections of balloon profiles on to axial plane.

profiles for $\gamma = 0$ (no air drag) with the other values, it becomes evident that, while the air drag is small, the balloon profiles are little affected by the air drag except near the nodes. In particular, the maximum balloon radius seems unaffected by air drag. De Barr[17] found that, to a first approximation, the maximum balloon radius depends only on the yarn count and the ring radius.

It can be seen from Figure 8.13 that, instead of a nodal point, the air drag causes the balloon profile to narrow to a minimum radius referred to as a *neck*. One way of explaining the reason for this is that, at any element of the balloon length, work is required per revolution to overcome the air drag on the yarn length from the lappet guide to the element. This work is equal to the product of the tangential component and the circumference of the circular path described by that element. Hence, where a nodal point would occur, there has to be a minimum radius. The neck is, however, smaller than the ring bobbin radius, and contact between the two causes the balloon to collapse.

It is evident from Figure 8.13 that, in causing a neck to be formed, the air drag extends the wavelength, i.e., the value of z/P that equals 1/2 λ. This would tend to support De Barr's proposition that the sinusoidal waveform of Equation 8.45 gives a better representation of spinning balloons or, more correctly, their projections onto the axial plane.

8.3.3 Determination of Ring Spinning Balloon Profiles Based on Sinusoidal Waveforms

Figure 8.14 shows a range of sinewaves obtained by De Barr's simplified approach, from which the profile of a stable balloon can be determined for known values of balloon height, H, and ring radius, R.[17] Using the nondimensional form, the balloon shape is given by that curve on which the point H/P (= z/P), R/P (= r/P) lies. As indicated, R and H define the angle β ($\tan\beta = R/H$) between the common axis and the line linking the apex (the lappet guide) and the point H/P, R/P. The importance of β is that it indicates the possible range of balloon profiles for a particular spinning geometry. Balloon profiles predicted by De Barr's approach are shown in Figure 8.15 along with observed values of maximum radii, and there is sufficiently good agreement to make this method of practical use.[17]

From Equation 8.23, P is dependent on the spinning tension, the traveler speed, and yarn count, and changes in these parameters will lead to a change of position of the point H/P, R/P along the line $\tan\beta$. The actual balloon size will depend on P; the smaller this value, the greater the maximum radius. For any combination of H and R, there is a minimum P below which a neck is formed.

Since P will fluctuate as the parameters of Equation 8.23 fluctuate, it is important that the point H/P, R/P be carefully chosen. It can be seen from Figure 8.14 that, in the region just below the maximum radii, the profiles come close together. In this region, quite small changes in P can result in significant changes in the balloon profile and maximum diameter. To produce the largest possible package for a given ring radius, yarn count, and tension, the point H/P, R/P would be chosen close to the boundary for a necked balloon formation. However, allowance should be given for fluctuation that would reduce P and thereby cause balloon collapse.

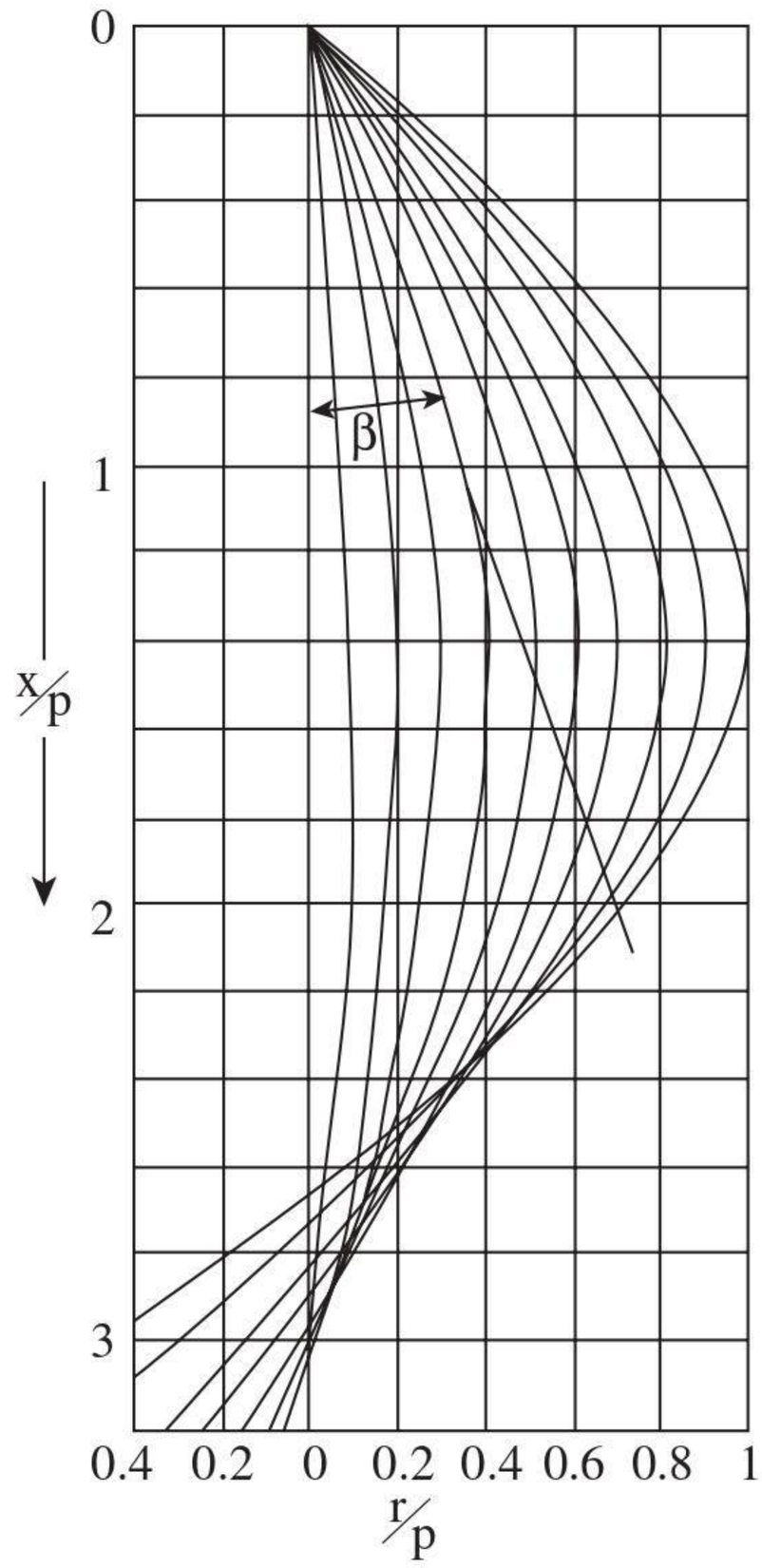

FIGURE 8.14 Determination of balloon shapes in ring spinning.

8.3.4 Effect of Balloon Control Rings

It can be seen from Figure 8.14 that, with a given spindle speed, yarn count, and R, for balloon collapse to be avoided with increased H, P must be increased to maintain a constant H/P. This means increasing tension T_O. For any yarn, there will be a limit beyond which end breaks occur. In Chapter 6, it was explained that the use of balloon control rings to divide the balloon length into two or more parts enables H to be increased without excessively increasing T_O. Thereby, larger ring-spinning packages can be made. For optimal effectiveness, control rings are of equal internal diameter to that of the ring, and they must be suitably positioned to keep balloon collapse from still occurring. The simple example is of a single control ring positioned such that two half-wavelengths of equal maximum radius are obtained (see Figure 8.16[17]).

The increased balloon length resulting from the use of control rings, and the friction between the length and the rings, result in an increased winding tension. This means that, to obtain a specific level of winding tension for a firm package, a lighter traveler can be used, which reduces the frictional drag of ring on traveler and, consequently, the spinning tension, T_S. A further advantage of control rings is that they damp tension fluctuations reaching the spinning zone, and such fluctuations could cause end breaks.

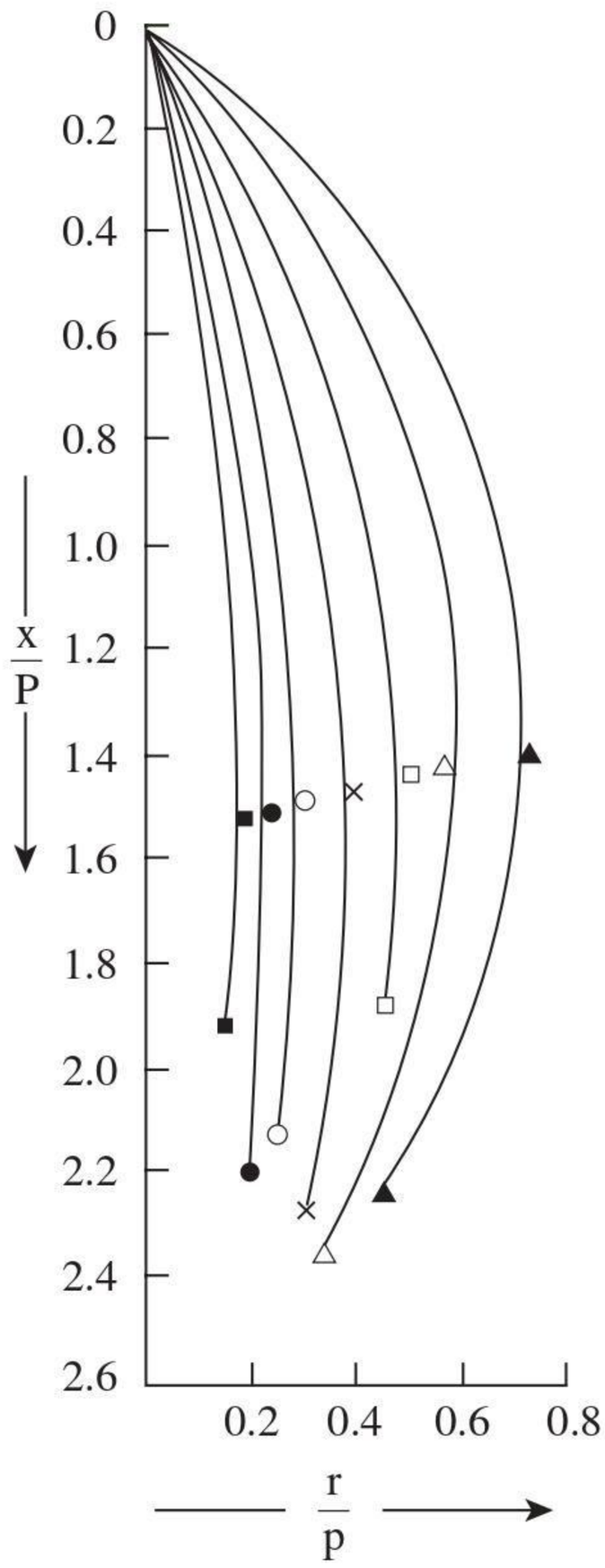

FIGURE 8.15 Observed and calculated balloon shapes.

8.4 TENSIONS AND BALLOON PROFILES IN THE WINDING PROCESS

We have seen above that, in ring spinning, the tensions in balloons are largely determined by the frictional drag of the ring on traveler, and these tensions determine the balloon profiles. In winding off yarns from ring bobbins, balloon tensions are essentially determined by the balloon shape.

8.4.1 Yarn Tensions during Unwinding from a Ring-Spinning Package

In Chapter 7, the path of the yarn from the ring package to cylindrical or conical bobbins was described, and the tension changes that occur during the process were explained. It is appropriate here to reconsider these tension changes with regard to the unwinding balloon profiles. The terms used have been already explained in the earlier chapter.

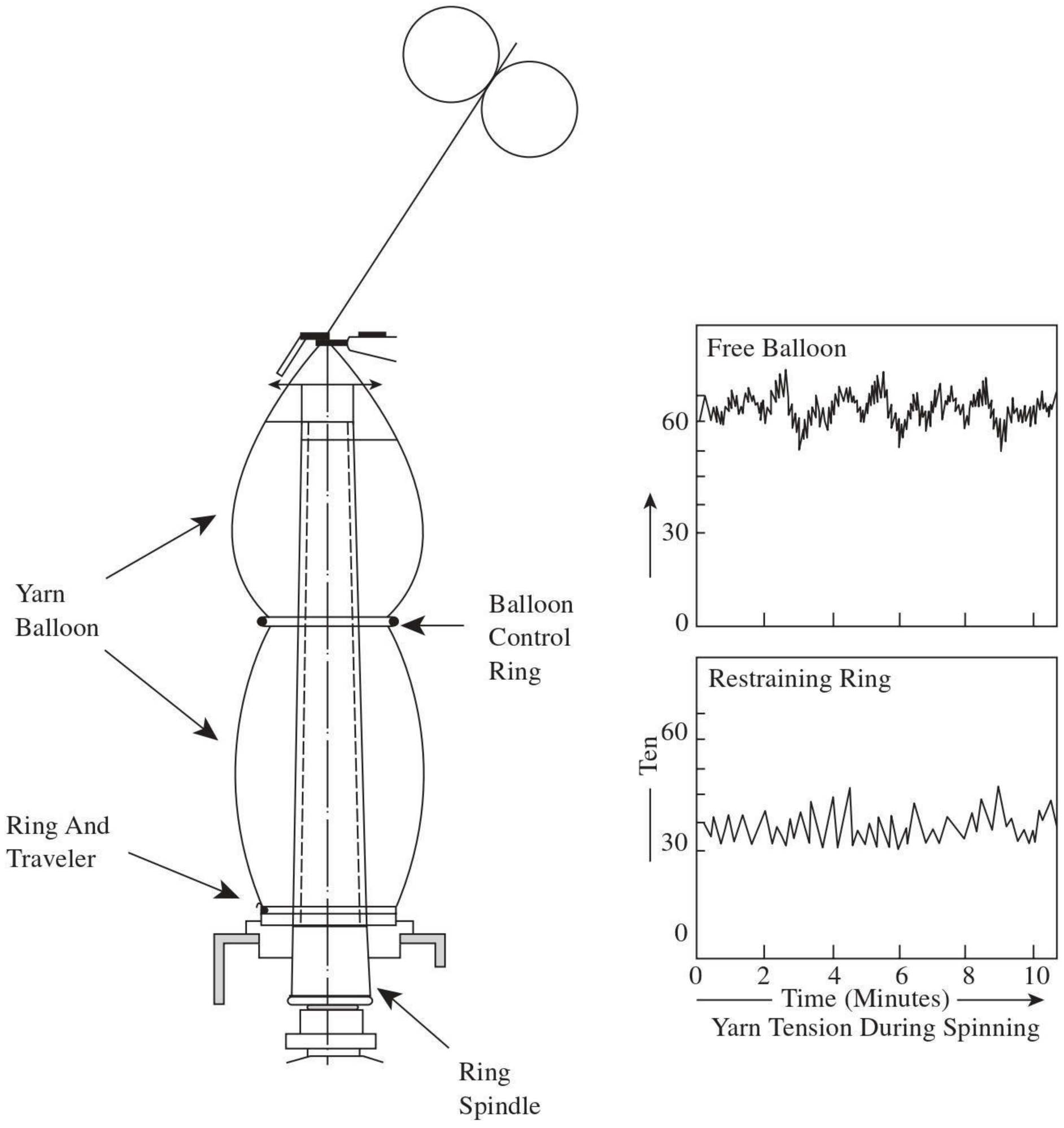

FIGURE 8.16 Effect of balloon control rings.

Figure 8.17 depicts the instantaneous profile of the balloon at the start of over-end unwinding. The point of unwinding is the contact point of the balloon with the package. In the early stages of unwinding from a cop-build ring package, the yarn length between the point of unwinding and the thread guide will form either a single-node or a multiple-necked balloon. The number of necks formed will depend on the speed of unwinding, the height of the tread guide above the package (i.e., H), the balloon height, the yarn count, and the package radius, R_P. Whereas the amplitude of the waveform is constant, the radius of the neck decreases toward the thread guide. As explained earlier for ring spinning, it is the tangential component of tension induced in the yarn by air drag that is responsible for a neck forming rather than a true node. This component of tension increases with distance from the thread guide down to the package. Consequently, the radius of each neck becomes greater than the preceding one when moving down the thread line toward the package. Mack[5] has shown that the radius of the nth neck is n times the radius of the first. Figure 8.18 illustrates the situation for a typical three-neck profile.

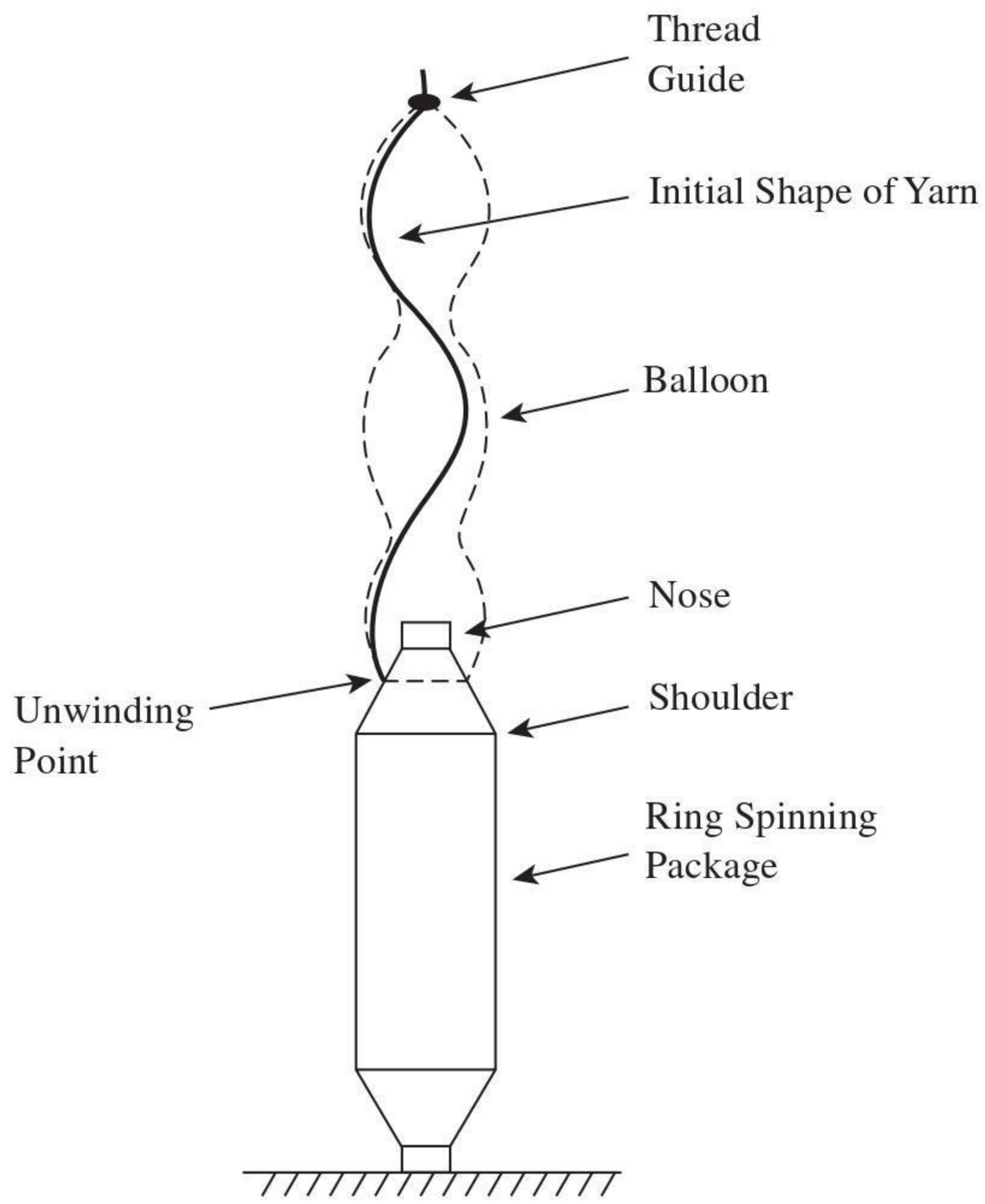

FIGURE 8.17 Balloon profile at the start of unwinding from ring-spun yarn package.

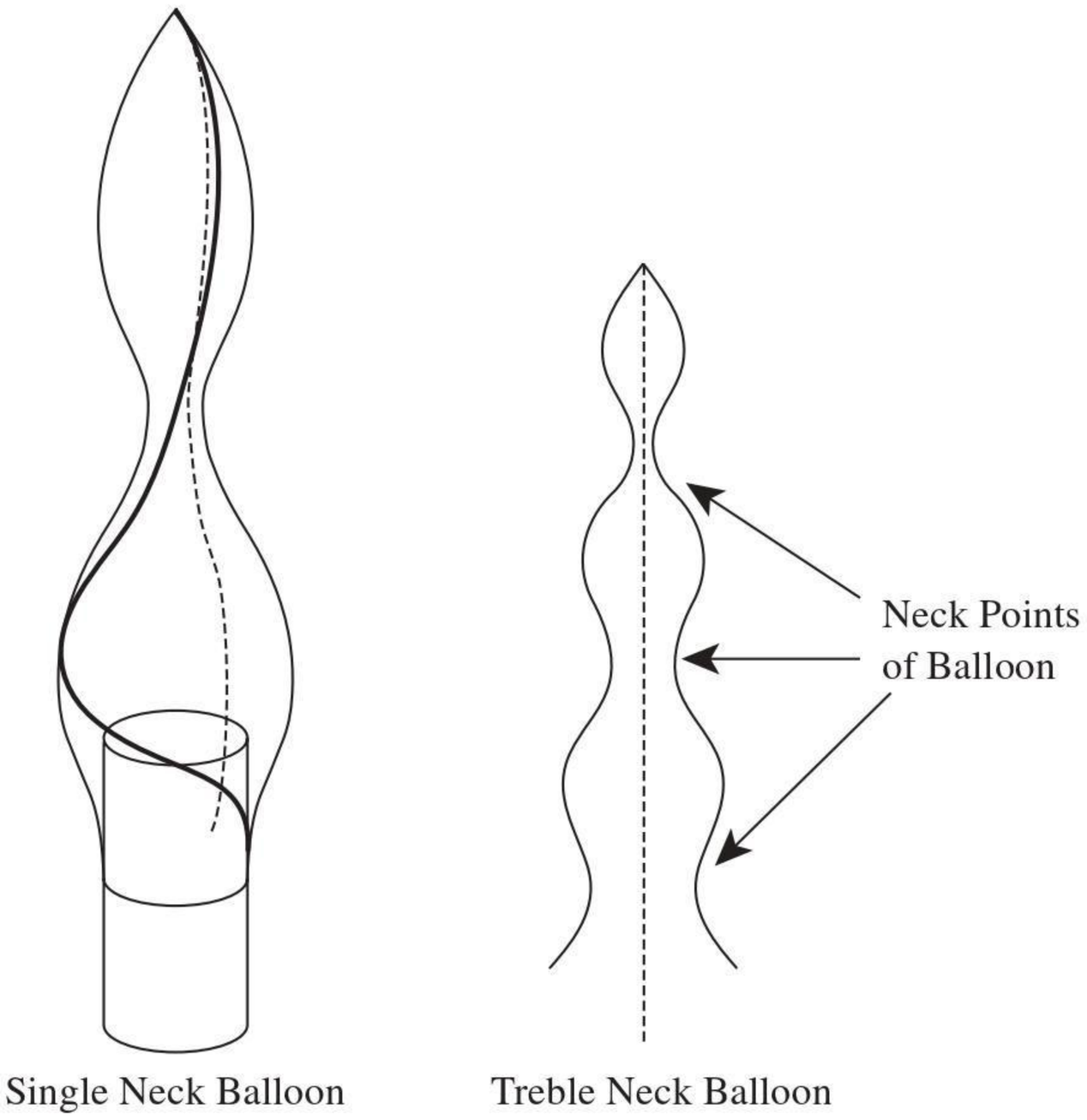

FIGURE 8.18 Treble-neck balloon profile.

The mean unwinding point of the cop-build package moves down the package length, from (a) to (f), etc., as the removal of the yarn proceeds, and this increases H (see Figure 8.19). A point will be reached where the neck nearest the bobbin package (i.e., the package core) coincides with the bobbin diameter, and a two-neck profile results. With further yarn withdrawal, the unwinding point moves within the base region of the bobbin, and a single-node balloon is formed.

Figure 8.20 indicates the changes in the unwinding tension, T_U, measured above the thread guide. If T_O is the tension at the thread guide during the yarn withdrawal, Equation 8.3 applies, with T_U replacing T_S. The mean tension and the variation in tension are of importance. The high-frequency or short-term variation at the start of unwinding comes from fluctuations in H associated with the unwinding point traversing the short length from nose to shoulder of the package. The change from a three- to a two-neck profile corresponds a substantial increase in the balloon wavelength and causes the step increase ΔT_{O1} in the mean tension. The subsequent change to a single-node balloon causes the second step increase ΔT_{O2}. It is clear that, between the step changes, the mean tension increases continuously, but the rate of increase after ΔT_{O1} is higher, and the size of the fluctuations is much greater. Following the changes in the balloon profile, the contact point of the balloon length with the package is no longer also the unwinding point. The yarn length being uncoiled is now dragged over a section of the cleared bobbin surface prior to becoming part of the balloon length. The mean unwinding tension increases because of the frictional drag of the yarn on the bobbin surface.

The increased intension limits the maximum unwinding speed because of a high frequency of end breaks. Figure 8.20 also illustrates the use of computer control drive system, the Autospeed, which uses an optical sensor unit to determine the

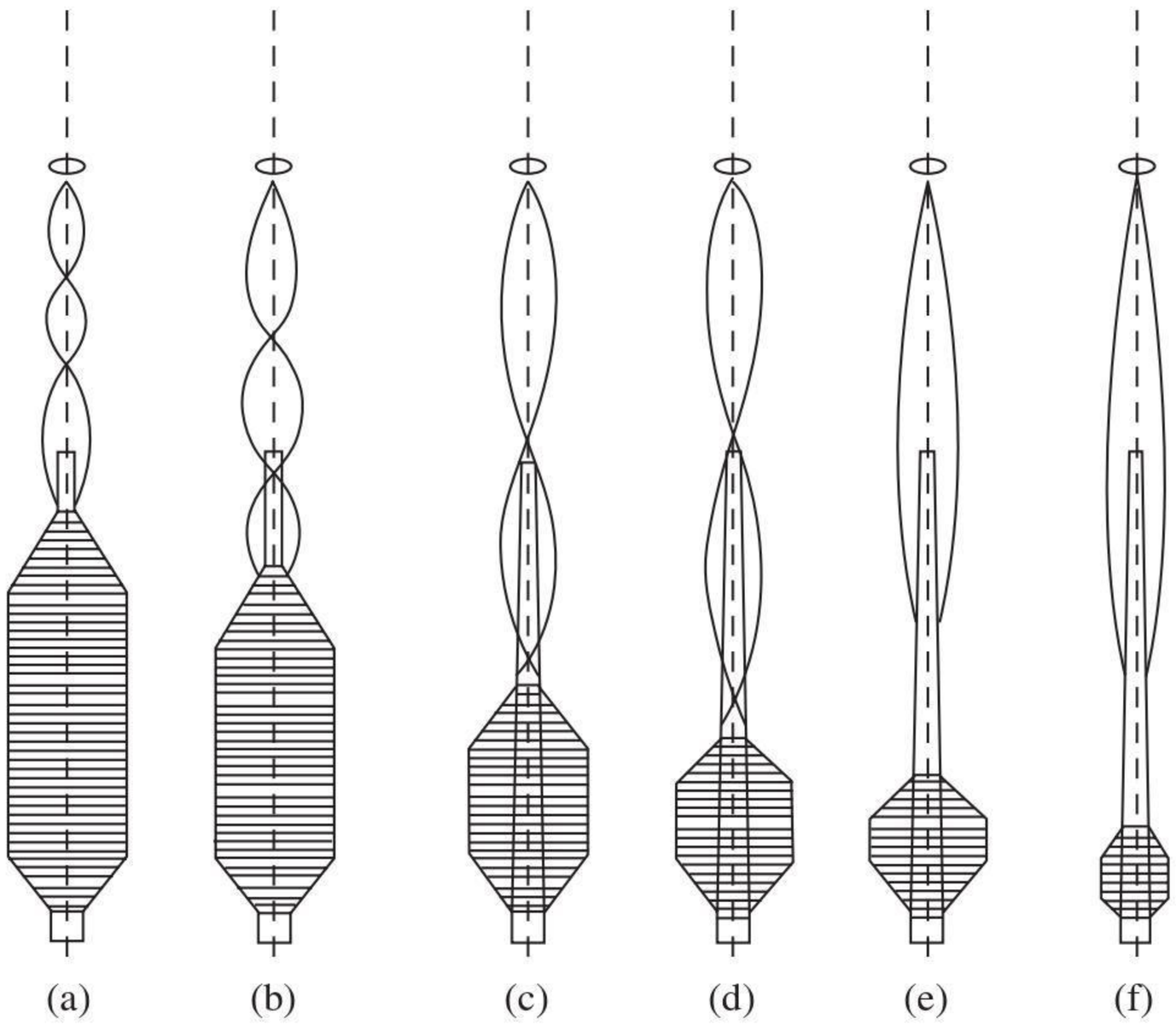

FIGURE 8.19 Changes in balloon profile during unwinding.

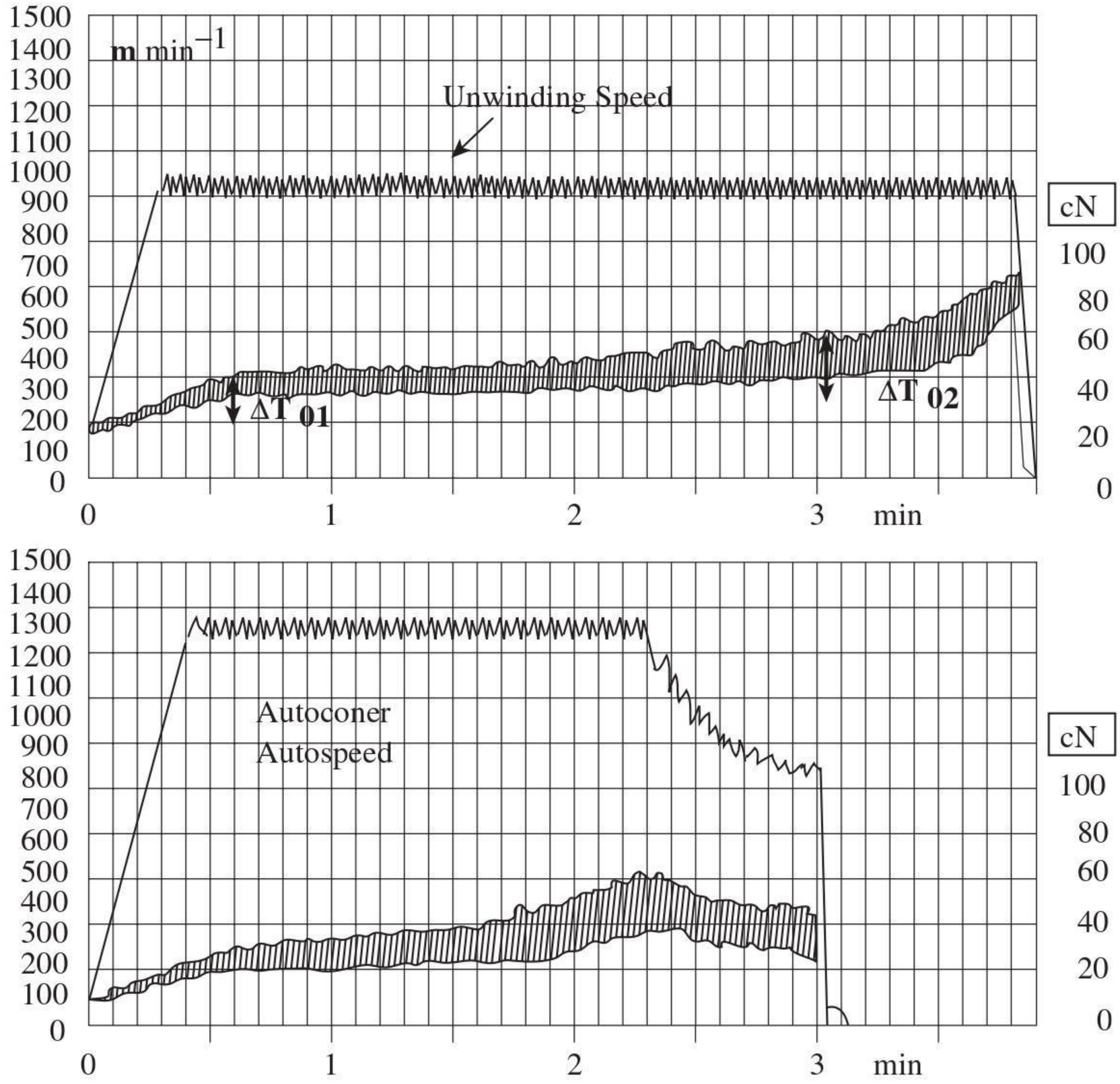

FIGURE 8.20 Changes in unwinding tension. (Courtesy of W. Schlafhorst AG & Co.)

amount of yarn on individual yarn packages and then adjusts the speed profile to prevent the step increase in tension toward the end of package unwinding. As shown, significantly higher unwinding speeds can be achieved.

Figure 8.21 illustrates the path taken by the yarn as it slides over the bobbin surface.[17] There is a gradual change in direction of the path on the bobbin to the direction in which a yarn element becomes part of the balloon. At the point of contact of balloon and bobbin, the angle of inclination, ϑ, of the yarn path on the bobbin surface to the tangent of the bobbin radius is therefore the same as that at the start of unwinding. The friction between yarn and bobbin maintains this equilibrium. Padfield[18,19] showed that the tension in the balloon at this contact point is largely due to this friction and is given by

$$T_F = 2\,(T_O - \frac{3}{2}mv^2)\,\sin^2\,\frac{1}{2}\vartheta \tag{8.50}$$

where v = the linear unwinding velocity of the yarn

In ring spinning, T_R is the tension in the yarn balloon at a similar position. In making a comparison with ring spinning, tension T_F and the tension resulting from the balloon profile have importance in how they relate to T_O and thereby T_U. It is therefore appropriate to consider now the tension due to the balloon profile and the associated forces.

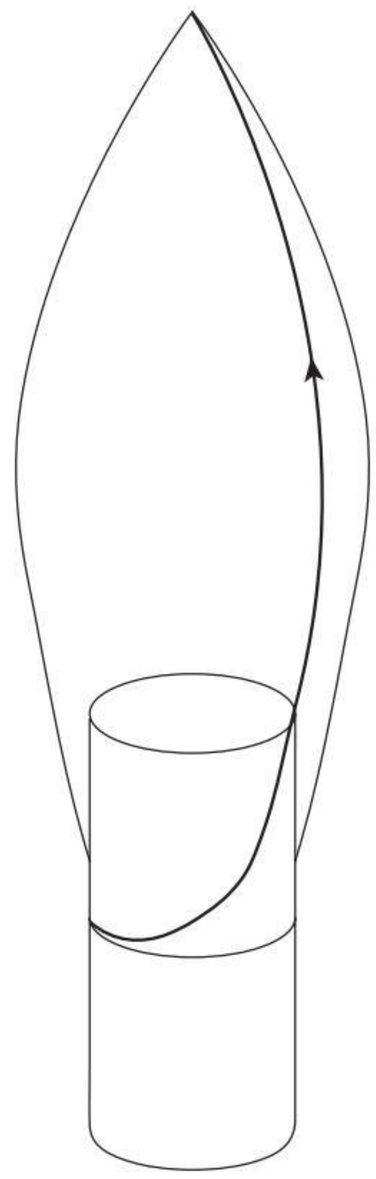

FIGURE 8.21 Yarn path on bobbin surface.

When an element of yarn is pulled from the yarn package through the thread guide, its rotational and translational kinetic energies change along the path. These changes are caused by forces that give rise to the yarn tension.

The early part of this chapter explained that, in moving from one radius to another, the change in kinetic energy of rotation is caused by Coriolis forces. With the high linear yarn velocities used in the winding process, the Coriolis forces are much greater than in ring spinning and now are not negligible. The balloon profile in winding depends, then, on the relative magnitudes of the air drag and Coriolis forces. For any yarn element of the balloon, the component of Coriolis force associated with the tangential component of velocity is greater than the air-drag force. However, the air-drag forces are cumulative from one end of the balloon to the other, whereas the Coriolis forces above and below the maximum radii are of opposite signs. At the package, therefore, the tangential component of tension is effectively the total air drag on the balloon. Near the thread guide, the Coriolis forces will be greater than the air-drag forces, and each yarn element of the balloon will lag behind the element above it. The reverse occurs near the package, where air-drag forces dominate (see Figure 8.21).

The kinetic energy of rotation of the yarn is zero on the package and, effectively, also at the thread guide. Therefore, there is no change in this kinetic energy in the process, so Coriolis forces do not contribute to T_O, even though they influence the tension in any considered yarn element of the balloon.

The translational kinetic energy results from the force required to accelerate each yarn element from its stationary position on the package to the linear velocity, v, along its length as it leaves the package. This force is provided by a component of tension in the yarn of magnitude $1/2\, mv^2 \sec \vartheta$, m being the mass of the element, and is constant over the length of the yarn.

With respect to the above points, we can say that the pulling of the yarn through the thread guide causes work to be done to

- Accelerate the yarn to the unwinding velocity (i.e., the linear velocity v)
- Overcome the frictional drag of the package on the yarn
- Overcome air-drag on the balloon length

The rate at which the work is done is given by vT_O. The work rate against air drag is

$$\int_0^L 1/2\rho_A \xi d\, r^3 \omega^3 dl \tag{8.51}$$

where L = total length of yarn in the balloon
r = radius of rotation of the element dl

Since $v = R_P\omega$, the air drag contributing to the yarn tension is

$$T_A = \frac{mv^2 \rho_A \xi d}{2mR_P^3} \int_0^L r^3 dl \tag{8.52}$$

The tension at the thread guide T_o is the sum of the contributions of friction and drag (Equation 8.50), air drag T_A, and the acceleration of the yarn, 1/2 mv^2 sec ϑ. Thus,

$$T_O = mv^2 \sec\vartheta \left\{ \left[\frac{\rho_A \xi d}{2mR_P^3} \right] \int_0^L r^3 dl + 2(T_O - 3/2mv^2)\sin^2 1/2\vartheta + 1/2 \right\} \tag{8.53}$$

8.4.2 Unwinding Balloon Profiles

The description given earlier of the three-neck balloon profile was a specific example. To determine the balloon profile of the unwinding yarn by performing a rigorous analysis of the acting forces requires the inclusion of the parameters for Coriolis forces in the differential equations of motion given in Table 8.1, and then with boundary conditions specific to the case of over-end unwinding, solving the equations numerically. A less exact but much simplified alternative is to use De Barr's approach[18] of the approximation of the sinusoidal projection on to the axial plane (z–r plane). In this case, the balloon profile for unwinding will correspond to the largest profile associated with given values of R_P/P and H/P.

REFERENCES

1. Escher, R., Theory of the ring spindle, *Der Civiingineur,* 1883, 29, 448.
2. De Barr, A. E., A descriptive account of yarn tensions and balloon shapes in ring spinning, *J. Text. Inst.*, 49, T58–T88, 1985.

3. *Wool Research*, Vol. 6, WIRA/British Textile Technology Group, Leeds, U.K.
4. Mack, C. and Smart, E. J. L., *J. Text. Inst.*, 45, T348, 1954.
5. Mack, C., Theoretical study of ring and cap spinning balloon curves (with and without air-drag), J. *Text. Inst.*, 44(11), T483–T498, 1953.
6. Lisini, G. G., Toni, P., Quilghini, D., and Campedelli, V. L. D., A comparison of stationary and non-stationary mathematical models for the ring-spinning process, *J. Text. Inst.*, 4(83), 550–559, 1992.
7. Crank, J., A theoretical investigation of cap and ring spinning systems, *Text. Res. J.,* 23, T266, 1953.
8. Crank, J. and Whitmore, D. D., The influence of friction and traveller weight in ring spinning, *Text. Res. J.*, 24, T1006, 1954.
9. Crank, J. and Whitmore, D. D., Balloon diameter and thread tensions calculated for different cap spinning conditions, *Text. Res. J.,* 23, T657, 1953.
10. Gregory, J. and Smart, E. J. L., The ballooning thread apparatus, *J. Text. Inst.*, 46, T606, 1955.
11. Lindner, G., *Leipziger Monatscherft fur Textil Industrie,* 213, 1910.
12. Grishin, P. F., *Platt's Bulletin*, 8, 161, 240, and 333.
13. Honneger, E. and Fehr, A., Effect of accessory influences on ring spinning of cotton and spun rayon, *J. Text. Inst.,* 38, 353, l947.
14. Bracewell, G. M. and Greenhalgh, K., Dynamical analysis of spinning balloon, *J. Text. Inst.*, 44, T266, 1953.
15. De Barr, A. E., The physics of yarn tensions and balloon shapes in spinning, winding and similar processes, *J. Text Inst.,* 51, T17, 1960.
16. De Barr, A.E., The role of air drag in ring spinning, *J. Text Inst.,* 49, T58, 1958.
17. De Barr, A. E., A descriptive account of yarn tension and balloon shapes in ring spinning, *J. Text. Inst.*, 49, T58–T88, 1958.
18. Padfield, D. G., A note on friction between yarn and package, *J. Text. Inst.*, 46, T71, 1955.
19. Padfield, D. G., The motion and tension of an unwinding thread, I, *Proc. Royal Soc.*, A245, 382, 1958.